LAPPEENRANTA UNIVERSITY OF TECHNOLOGY

School of Engineering Science

Degree Program in Chemical and Process Engineering

MASTER'S THESIS

ADSORPTION OF RARE EARTH ELEMENTS ON NOVEL "Mg-Al LAYERED DOUBLE HYDROXIDE WITH GUM ARABIC"

1st Examiner: Prof. Mika Sillanpää

2nd Examiner: Sidra Iftekhar

Author: Waqar Ahmed Naseer

Dated: 18.10.2018

ABSTRACT

Lappeenranta University of Technology
Chemical Engineering Department
Degree Program in Chemical and Process Engineering
Waqar Ahmad Naseer

ADSORPTION OF RARE EARTH ELEMENTS ON NOVEL "Mg-Al LAYERED DOUBLE HYDROXIDE WITH GUM ARABIC''

Master's Thesis
2018

72 pages, 23 figures, 9 tables
1st Examiner: Prof. Mika Sillanpää

2nd Examiner: Sidra Iftekhar

Keywords: Rare earth metals; Adsorption; Bio-Nano-Composites; Layered double hydroxide; Gum Arabic; Isotherms; Kinetics

Abstract

In the last few decades, the demand for rare earth elements has increased, as there have been further discoveries for their use. Rare earth elements are used for very specific applications and can be extracted from different ores and wastes. Conventional methods for their extraction are not economical or eco-friendly. Moreover, the currently existing technologies have environmentally unfriendly aspects.

Adsorption is a simple and economical approach for recovering rare earth elements. A selective choice over the adsorption material can make the adsorption process green and sustainable.

The following research is based on finding an appropriate biodegradable adsorbent for the removal of rare earth elements. The objectives of the research were to synthesise an efficient nanocomposite from the biodegradable source. Mg-Al layered double hydroxide (LDH) nanocomposite with gum Arabic, gives promising results for recovering **Sc, La, Nd, Eu, Ce and Y** from aqueous solutions.

The theoretical part of the work covers information about the properties, behaviour, demand and different ideas of the adsorption process. The experimental part comprises two parts: the first focus on different approaches to look for a bio nanocomposite adsorbent and the second part is about the characterisation and effect of the initial conditions on the adsorption process. The effect of different variables, such as time, initial concentration, dose, initial pH and temperature, were investigated in detail and the optimum conditions were enlisted.

Furthermore, the results of the research prove that Mg-Al G.A. LDH is a good adsorbent for removing rare earth elements. It has higher removal and, therefore, it can be used as an efficient adsorbent for future pilot and industrial plants.

ACKNOWLEDGEMENTS

Firstly, I owe my deepest gratitude to Professor Mika Sillanpää for giving me such a great opportunity to work in an exciting and innovative environment. Throughout the research, the staff members have been very helpful and supportive.

I would also like to thank Sidra Iftikhar who has supported me and advised me throughout. I have been comfortable working with her, and her calm and professional attitude has encouraged me along every step of the way.

I am grateful to Dr Varsha Srivastava and Deepika Ramasamy who have helped me run the ICP samples and provided me with their assistance in the laboratory on different occasions.

The working environment in the DGC lab has been very motivating. All the people in the Lab are helpful and cooperative and that always made me enthusiastic and energetic while conducting my research.

Lastly, special thanks to my family for the support they provided me through their words and prayers.

Moreover, I'm keen to make some more discoveries in the future and so I will try to invent some truly great things for improving life on Earth.

Waqar Naseer

18/10/2018

TABLE OF CONTENTS

LIST OF FIGURES

LIST OF TABLES

LIST OF SYMBOLS AND ABBREVIATIONS

LDH	Layered double hydroxide
G.A.	Gum Arabic
REE	Rare earth element
REEs	Rare earth elements
REM	Rare earth metals
REO	Rare Earth Oxides
LREEs, HREEs	Light and Heavier, Rare earth elements
FCC	Fluid catalytic cracking catalyst
SX	Solvent extraction
HFO	Hydrous ferric oxide
D-R	Dubinin-Raushkevich
BCD	By-pass cement dust
MSR	Malt spent root
FTIR	Fourier Transform Infrared Spectroscopy
XRD	X-Ray Diffractometer
TEM	Transmission electron microscopy
SEM	Scanning electron microscopy
DLS	Dynamic light scattering
TGA	Thermal gravimetric analysis
MNHA	Magnetic Nano-hydroxyapatite
EDTA	Ethylenediaminetetraacetic acid
DTPA	Diethylenetriaminepentaacetic acid
Alg-PGA	Alginate- Polyglutamic acid
CNPs	Carbon Nano Particles
PAN	1-(2-pyridylazo) 2-naphthol
ACAC	Acetylacetone
DI	De-ionised
APTES	3-aminopropyl triethoxysilane
APTMS	3-aminopropyl trimethoxysilane
MTM	Trimethoxymethylsilane

TMCS	Chlorotrimethylsilane
Nm	Receptor site density
c1/2	Concentration at half saturation
A	Temkin isotherm equilibrium binding constant
b	Temkin isotherm constant
C_o	Initial concentration in aqueous media
C_e	Equilibrium concentration
q	Adsorption capacity, mg/g
q_e	Equilibrium adsorption capacity, mg/g
q_m	Maximum adsorption capacity, mg/g
k_1	Pseudo-first-order rate constant
k	Pseudo-second-order rate constant
k_i	Intra-particle diffusion rate constant
k_f	Film diffusion rate constant
K_L	Langmuir isotherm constant
K_F	Freundlich isotherm constant
K_C	Thermodynamic equilibrium constant
n	Partial order for adsorbent
ΔG^o	Gibbs free energy (J/mol/K)
ΔS^o	Entropy (J/mol/K)
ΔH^o	Enthalpy (kJ/mol)
R	Universal gas constant, 8.314 J/mol K
R^2	Coefficient of determination
T	Absolute temperature, K
t	Time, min

1. INTRODUCTION

1.1 BACKGROUND

Rare Earth Elements (REEs) are lanthanide series from atomic number 57 to 71, including scandium and yttrium. REEs are highly valuable elements of similar properties which are applicable for use in various fields from mobile phones, wind turbines, cancer diagnosis and more. Their unique electronic structure makes them useful for electronic applications such as magnetism, cameras, computer drives, LED lights and other electronic devices (Bradley et al., 2014).

REEs are in fact not so rare in the earth crust compared to some other ores, but their occurrence in the mineable ore is very low. Most of the REEs ores contain much lower amounts and, therefore, cannot be profitably extracted. Currently, China is the leading producer of REEs in the world with nearly 90% of the global production. Present production methods consider concentrating the ores before extracting REEs. These methods are inefficient and are comparatively not so economical. Hence, there is a need to devise new methods which are greener in perspective and economically sustainable (Voncken, 2016).

Adsorption is one economical and efficient way for the uptake of REEs. It is green, sustainable and a rather straightforward approach to extract REEs from very low concentrations. The present paper's research targets the idea of making REEs extraction greener and sustainable by using biodegradable sources for adsorption (Voncken, 2016).

In the past few decades, Layered double Hydroxide (two-dimensional brucite layers of positively charged mixed metal ions) has gained a lot of attention in the world because of their enormous applications as adsorbents and carrier materials. LDH is an inherently great adsorbent and can adsorb even very low amounts quickly and efficiently. Through this study, it has been revealed that Mg-Al-G.A. LDH nanocomposite works efficiently for extracting REEs from liquid solutions. It works with an even lower dose and lower concentrations and, therefore, it is a promising adsorbent for REEs extraction.

1.2 OBJECTIVES OF RESEARCH

- To find an appropriate nanocomposite adsorbent utilising biological base i.e. bio-waste, starch, cellulose, gum Arabic and others; which is workable to adsorb REEs.
- To evaluate the adsorbents based on different modifications.
- Obtain basic data on adsorption.
- To look for the best-optimised conditions for adsorption.
- Study the adsorption for different initial conditions of time, dosage, concentrations, pH and temperature.
- Characterise the adsorbent using different instruments, such as FTIR, XRD and TEM

1.3 RESEARCH LAYOUT

The overall research was based on a six-month period which includes theoretical work, practical work and thesis writing. The research includes looking for literature and then hunting for different ideas about making workable bio nanocomposites for REEs adsorption. The second approach was to characterise the adsorbent and finally optimise the adsorption process. All of the theoretical and practical work was carried out in "DGC Lab in MIKKELI".

At first, to make a workable adsorbent for REEs, several experiments were conducted with different biomaterials including starch, cellulose, pectin, gum Arabic, κ-Carrageenan etc. Many approaches and different substitutes were tried in order to formulate bio nanocomposites i.e. metal oxides incorporated with biopolymers, co-precipitation of metal salts with bio-compounds and layered double hydroxide with +2 and +3 metal salts incorporated with biopolymers etc. All of those adsorbents were tested through all the initial characterisation to preliminary tests, and the results were compared in order to look for the best working option. Note that the results from the initial research are not reported in the following thesis and only the results with workable adsorbent are mentioned below.

The results from the preliminary test suggested that Mg-Al G.A. bio nanocomposites provided a significant amount of adsorption and can be used to remove REEs. After preliminary tests, further analyses were carried out to analyse the adsorbent and the best adsorption conditions.

2. RARE EARTH ELEMENTS

2.1 REEs GENERAL INTRODUCTION, PROPERTIES & COMMON USES

Rare earth elements represent the Lanthanide series, so-called transition metals, which makes the bottom of Mendeleev's periodic table. It's a group of 15 elements with very close properties which make them hard to separate from each other. Yttrium and scandium are two other metals which are also included in the REE series because of their similar properties as of other REEs. Furthermore, REEs are divided into lighter (LREEs) and heavier (HREEs) (U.S. EPA, 2012).

REEs (La-Lu) are f block elements, meaning their outmost electrons are positioned in f-orbitals. Since f-orbitals have 7 sub-orbitals, each of them can be filled with two electrons and, as a result, there can be 15 different ways of putting electrons in these subshells. That is why most of these elements possess quite the same properties. Lanthanides have an oxidation state of +3 except cerium +4 and europium, ytterbium and samarium can also go to the +2 oxidation state. Yttrium and Scandium both have the +3 oxidation state (Voncken, 2016).

The common properties of REEs include silvery or silver-grey surface, high lustre but vanish in the air quickly, higher ability to conduct electricity, readily forms complexes when dissolve to make solutions, present together in mineral ores with common oxidation state +3 (Voncken, 2016).

For the present study, six REEs are considered to demonstrate the adsorption phenomenon, which includes 4 lanthanides (LREEs) Lanthanum, Cerium, Neodymium, Europium along with Scandium (LREE) and Yttrium (HREE). A brief overview of these elements is explained below.

Lanthanum (La): Represents the lanthanide series, atomic number 57 and an atomic mass of 139. Its silvery shiny metal which losses rapidly with air exposure. Lanthanum is present in different mineral forms like monazite, cerite, biotite, apatite, pyroxene and feldspar. It is found mostly along with cerium and represents one of the abundant REE. Lanthanum is utilised in the form of alloys or in other chemical derivatives i.e. oxides, carbonates etc. The applications of Lanthanum include Nickel-lanthanum alloy to store hydrogen and their use as hybrid batteries for cars, La_2O_3 in glass industry to improve optical properties, Catalyst in catalytic cracking of hydrocarbons etc. (jlab.org 2017).

Cerium (Ce): Atomic number 58 and atomic mass 140 with variable oxidation states of +3 and +4, it represents the most abundant element of REEs. Presently it is obtained through solvent extraction process from monazite mineral ($CePO_4$). In pure form, it can be ignited if contacted with a sharp body, but its derivative products can be used safely i.e. in the form of nitrates or chlorides etc. Common uses of cerium include; uses as carbon arc lights for projector lights, flints material for lighters, the catalyst for the petroleum industry, cerium oxide is a component for walls of ovens and utilised for glass industry to polish and to remove colors form glass etc. (jlab.org 2017).

Neodymium (Nd): Atomic number 60 and atomic mass 144, it was discovered by German chemist Carl F. Auer von Welsbach in 1885. Neodymium is also extracted from REEs rich mineral monazite, through an ion exchange process. It is recognised from its strong paramagnetic properties and its applications in the electronics industry. Hence, most commonly utilised as permanent magnets in the form of an alloy with iron and boron, which extend its applications in electronics i.e. microphones, headphones, speakers etc. Other common uses include windscreen wipers, wind turbines, in the glass industry for special glass materials, as a catalyst for petrochemical industries and many more (jlab.org 2017).

Europium (Eu): Atomic number 63 and atomic mass 152, was first discovered by French chemist Eugène-Anatole Demarçay in 1896, who found europium in an associated form with samarium. The recent process uses ion exchange to recover europium from monazite sand minerals. It is the most reactive element among all the REEs. Although there are no industrial applications it is utilised in different sectors for making lasers form doped plastics, in television as red phosphor, used in euro currency notes because of its red luminance under UV light, applicable in the nuclear industry to absorb neutrons etc. (jlab.org 2017).

Scandium (Sc): Atomic number 21 and atomic mass 45, it is known from its variable states of +3, +2 and +1. It is included in REE series because of its presence in other lanthanides minerals. Moreover, its properties more resemble to yttrium and other REEs rather than elements like aluminium or titanium (Voncken, 2016).

Scandium was first discovered by a Swedish chemist, Lars Fredrik Nilson, in 1879. The extractable mineral sources of scandium include; thortveitite, bazzite and wiikite, but

mostly it is taken as a by-product from uranium refinery. Common uses are alloys of scandium and alloys used in sports equipment manufacturing i.e. baseball bats, to produce high intensity lights; scandium iodide is incorporated in mercury lamps to produce sun like lights etc. (jlab.org 2017).

Yttrium (Y): Atomic number 39 and atomic mass 89, it is considered as the heavy rare earth element. It was first found by Johan Gadolin, a Finnish chemist, in 1789, while studying REEs mineral gadolinite. Yttrium is a soft, silvery metal obtained from monazite sand which is the main source of Yttrium along with bastnaesite and Xenotime (rsc.org 2017).

Metallic yttrium does not have many applications for its compounds. Yttrium oxide is used to produce red phosphor with europium. Iron-yttrium garnets are utilised as microwave filters in communication systems and aluminium-yttrium garnets are used as replicable diamond jewellery (jlab.org 2017).

Some other applications of yttrium are: strengthening agent in different alloys, as a catalyst in polymerisation reactions, Y_2O_3 is used to make glass lenses heat and shock absorber, utilised to make superconductors, its radioactive isotopes can treat liver cancers, etc. (rsc.org 2017).

2.2 PRODUCTION &DEPOSITS OF REEs

REEs are not rare on Earth, but most of them were present for years in the Earth's crust unseparated. Due to their similar properties, it makes it too difficult to separate them from each other (Hurst, 2010). Even though REEs are present extensively all over the globe, their production is limited to certain countries. China is the largest producer of REEs which provides nearly 90% of the REE production while Australia and the US are the 2nd and 3rd largest producers, respectively.

Globally, mineral deposits of REEs are present in Canada, China, India, Malawi, Russia, South Africa, Vietnam and the United States. The overall deposits on Earth amount to approximately 120,000,000 tons. China has most of the deposits of REEs totalling 44,000,000 followed by Brazil and Vietnam at 22,000,000. China also rules the world's largest production of REEs and produces almost 105,000 tons of REEs per year (USGS, January 2017).

Table 1: Worldwide REEs production and reserves (U.S. geological survey mineral commodity summaries, 2017)

	Mine Production		**Reserves**
	2015	2016	
US	5,900	--	1,400,000
Australia	12,000	14,000	3,400,000
Brazil	880	1,100	22,000,000
China	105,000	105,000	44,000,000
India	1,700	1,700	6,900,000
Malaysia	500	300	30,000
Russia	2,800	3,000	18,000,000
Vietnam	250	300	22,000,000
World total (approx.~)	130,000	126,000	120,000,000

World mine production of REEs has gone through different phases of growth. The first phase: from 1990 to 2006, where the growth has increased rapidly due to discoveries on their advanced uses. In 2007, where the production decreases due to the global financial crisis and in further production increases to a slightly slower rate. The production of REEs is directly dependent on the growing demand and uses. As the technology developed apart from their conventional uses as a catalyst, automobiles, phosphorus industry etc.; an increase in their uses developed in other technology as strong paramagnets for wind turbines, computer hard drives and in other fields. Hence, the rapid growth initiated in the early 21st century with a rapid growing world demand in the beginning and then finally settled to a steady rate later on (Goonan 2011).

The figure below graphically represents the trend of REEs production in the last few decades:

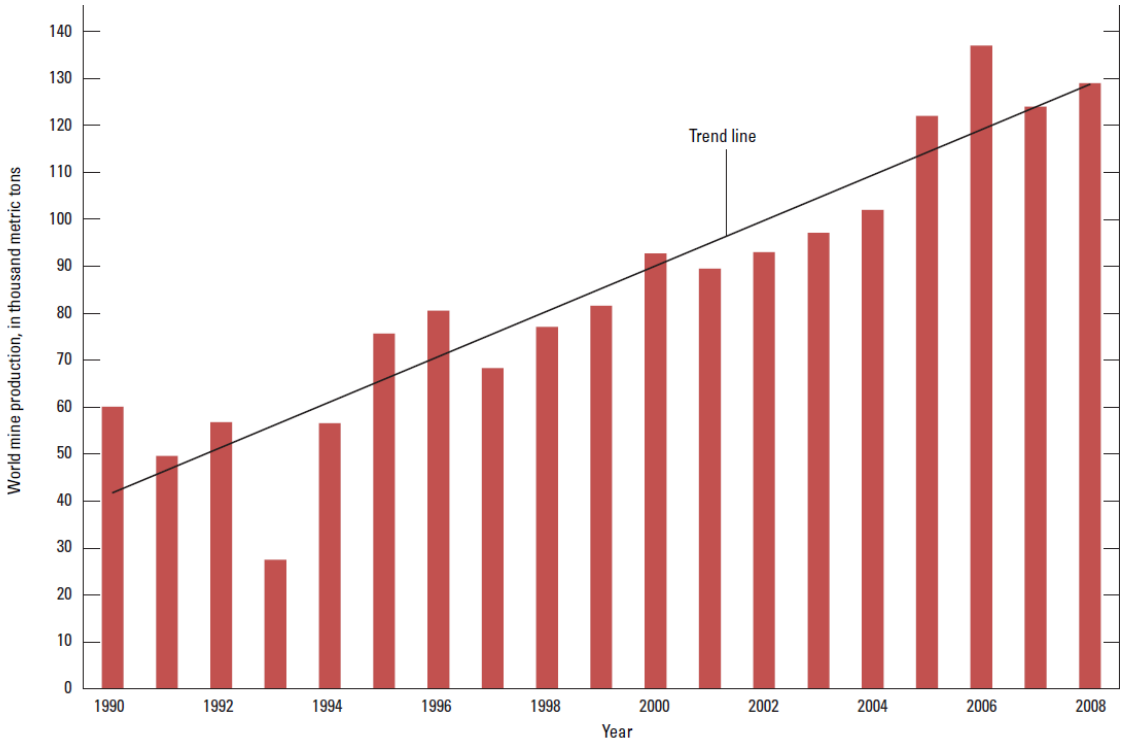

Figure 1: World mine production of rare earth oxides from 1990 to 2008. Data from Hedrick (1996–2009), Cordier and Hedrick (2010)

In 2016, many REEs' prices decreased due to an elevated production and global supply. China remains the leading country with 105,000 tons of REEs production in 2016. In September, China has exported 35,200 tons of REEs globally which is 50% more than the records from the year 2015. Similarly, REEs oxides derived from the concentrate mined in Australia was 6,290 by June 2016, which is 37% more than last year. Exploration efforts have also been continued in the area to develop REEs i.e. exploration and development assessments in the United States Bear Lodge, WY; Bokan Mountain, AK; Diamond Creek, ID; Elk Creek, NE; La Paz, AZ; Lemhi Pass, ID-MT; Pea Ridge, MO; Round Top, TX; and Thor, NV. Further projects are yet to start in Australia, Brazil, Canada, China, Finland, Greenland, India, Kyrgyzstan, Madagascar, Malawi, Mozambique, Namibia, South Africa, Sweden, Tanzania, Turkey and Vietnam (Gambogi, U.S. Geological Survey 2017).

2.2.1 REEs COMMON MINERALS TYPES

REEs can be found in different types of mineral sources; among this monazite, bastnaesite and xenotime are considered to be potentially extractable minerals. The first ever mineral

to be used for REEs extraction was gadolinite, whereas monazite was first used for the industrial production of REEs (Voncken, 2016).

The table below shows different types of potentially economical REEs mineral sources with their general formulas and REEs content.

Table 2: Potentially economical REEs mineral sources (Castor and Hedrick, 2006)

Mineral	**Formula**	**REE WT%**
Aeschynite	(Ln*,Ca,Fe,Th)(Ti,Nb)2(O,OH)6	36
Allanite (orthite)	(Ca,Ln)2(Al,Fe)3(SiO_4)3(OH)	30
Ancylite	SrLn(CO_3)2(OH)•H2O	46
Apatite	Ca5(PO_4)3(F,Cl,OH)	19
Bastnasite	*LnCO_3F*	*76*
Britholite	(Ln,Ca)5(SiO_4,PO_4)3(OH,F)	62
Cerianite	(Ce,Th)O2	81
Churchite	YPO_4•2H2O	44
Eudialyte	Na15Ca6(Fe,Mn)3Zr3(Si,Nb)Si25O73(OH,Cl,H2O)5	10
Euxenite	(Ln,Ca,U,Th)(Nb,Ta,Ti)2O6	~40
Fergusonite	Ln(Nb,Ti)O4	47
Florencite	LnAl3(PO_4)2(OH)6	32
Gadolinite	LnFeBe2Si2O10	52
Huanghoite	BaLn(CO_3)2F	38
Hydroxylbastnasite	LnCO_3(OH,F)	75
Kainosite	Ca2(Y,Ln)2Si4O12CO_3•H2O	38
Loparite	(Ln,Na,Ca)(Ti,Nb)O3	36
Monazite	*(Ln,Th)PO_4*	*71*
Mosandrite	(Ca,Na,Ln)12(Ti,Zr)2Si7O31H6F4	~65
Parisite	CaLn2(CO_3)3F2	64
Samarskite	(Ln,U,Fe)3(Nb,Ta,Ti)5O16	12
Synchisite	CaLn(CO_3)2F	51
Thalenite	Y3Si3O10(OH)	63
Xenotime	*YPO_4*	*61*

Yttrotantalite	(Y,U,Fe)(Ta,Nb)O4	~24
*Ln	Light rare earth elements	

Monazite is represented by the general formula $CePO_4$. The name comes from the Greek word "monazies", meaning "to be alone" because of the nature of its lonely presence and rare presence of deposits. Along with Ce, other REEs are also present in monazite which is mostly LREEs, i.e. La, Pr, Nd and Sm. Some very low fractions of Th and U are present but not enough concentrated to be considered as an extractable source (Voncken, 2016).

The figure below shows Monazite stone from Norway:

Figure 2: Monazite, Iveland Setesdal, Norway. From the collection of Naturalis Biodiversity Center, Leiden, Netherlands, Sample RGM412064 (Voncken, 2016)

Bastanaesite was first described by Swedish chemist Wilhelm Hisinger (1838), from Bästnasmine near Riddarhyttan, Västmanland, Sweden. Bastanaesite is represented by the general formula $Ce(CO_3)F$. Like Monazite, it is also considered as a source of LREEs with the exception that it does not contain Th or U. Therefore, the absence of U and Th make it one preferable source for the extraction of LREEs. Yttrium, the only HREE, is also quite commonly found in Bastanaesite rocks along with low proportions of other HREEs. Common occurring forms are hydroxyl bastnaesite or carbonates and found mostly in igneous rocks (Voncken, 2016).

The figure below represents Bastanaesite rock from California:

Figure 3: Bastnaesite (yellowish material), Mountain Pass California. Sample from the collection of Naturalis Biodiversity Center, Leiden, Netherlands, Sample ST 82224 (Voncken, 2016)

Xenotime was explained by Berzelius in a specimen from Hidra (Hitterø), FlekkefjordVest-Agder, Norway. The common formula for representing Xenotime is YPO_4. Xenotime, compared with monazite and bastnaesite, contains larger amounts of HREEs i.e. Y, Tb, Dy, Ho, Er, Tm, Yb and Lu. Most common occurring REEs include Dy, Yb, Er and Gd. Unlike bastnaesite, Xenotime contains some fractions of Th and U, depending on the source of mineral deposit. The most common occurrence of Xenotime is in pegmatites, Igneous Rocks and metamorphic rocks (Voncken, 2016).

The figure below represents Xenotime mineral rock from Madagascar:

Figure 4: Xenotime, Madagascar. From the collection of Naturalis Biodiversity Center, Leiden, Netherlands, Sample RGM412055 (Voncken, 2016)

The table below describes some typical compositions of monazite, xenotime, and bastnaesite minerals, monazite Ce and monazite La also bastnaesite Ce, bastnaesite La and bastnaesite Y simply represent their major rare earth element in each of them, respectively.

Table 3: Mineral compositions of monazite, xenotime and bastnaesite (Web mineral, 2014)

Element	**Monazite-Ce**	**Monazite-La**	**Xenotime-Y**
La_2O_3	16.95	33.95	-
Ce_2O_3	34.16	17.10	-
ThO_2	5.50	5.50	-
$P2O_5$	29.55	29.58	38.60
Nd_2O_3	14.01	14.03	-
Y_2O_3	-	-	61.40
TOTAL	100.17	100.17	100.00
	Bastnaesite-Ce	Bastnaesite-La	Bastnaesite-Y
La_2O_3	-	74.76	-
Ce_2O_3	74.90	-	-
Y_2O_3	-	-	67.24
CO_2	20.08	20.20	26.21
F	8.67	8.72	11.31
Total	100.00	100.00	100.00

2.3 DEMAND, MARKET TRENDS AND APPLICATIONS OF REEs

REEs have enormous applications and are recognised from their irreplaceable specific functional in consumer products. Conventional REEs usage for lighter flints has changed from 75% in 1950 to 20% in early 2000. This dramatic change is basically the reason for discoveries on their broad uses in products. Presently, REEs are used in areas of glass polishing industry, refinery and automotive catalysts, permanent magnets, metallurgical applications and many more (Castor and Hedrick, 2006).

Glass polishing and ceramics are the biggest consuming market of REEs. Cerium is a key component in the glass polishing industry. Along with the glass industry, the refinery catalyst and automotive sector consume a large amount of REEs. Production of REEs in

the 1980s has been readily affected by elevated use of cerium oxide in the automotive industry. Use of La in the refinery as a catalyst makes it one essential need for refinery processes. Although the use of REEs is used quite less in phosphorus and electronics, each sector itself represents a higher value product (Castor and Hedrick, 2006).

In 1960, color television products contained phosphorus based on yttrium and europium which lately were replaced by gadolinium and terbium. Presently, trichromatic florescent tubes increased the demand of REEs in the global market. Samarium-cobalt greater strength magnets revolutionised the whole REEs markets because of their applications in high quality headphones and electric motors. Lately, these high-cost Samarium-cobalt magnets were replaced by neodymium-iron-boron permanent magnets but they are still irreplaceable for high temperature applications (Castor and Hedrick, 2006).

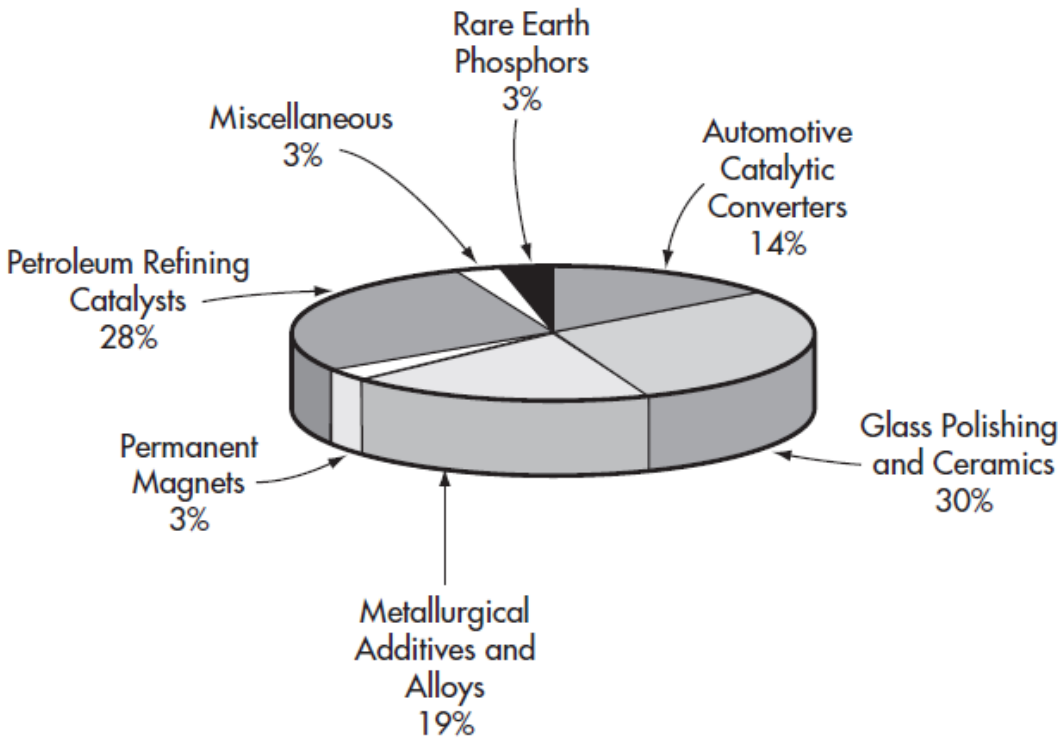

Figure 5: REEs Demand by Applications (Castor and Hedrick, 2006)

The worldwide demand for REEs has an increasing trend from the past few decades but the market is quite ambiguous and complex. Since all the REEs occur in a common mineral rock in constant proportions, so it is quite challenging to balance the production and demand. To solve this, each REE must be given a factor considering their presence in the

mineral ore to determine marketing equations. These equations become complex because of several other controlling parameters, i.e. operational costs for separation and purification, technological changes, stockpiling etc. (Castor and Hedrick, 2006).

The figure below further illustrates the price fluctuations in the REEs global market. The main governing factors are China's production limitations, stockpiling of REEs stock, unbalanced production and demand etc.

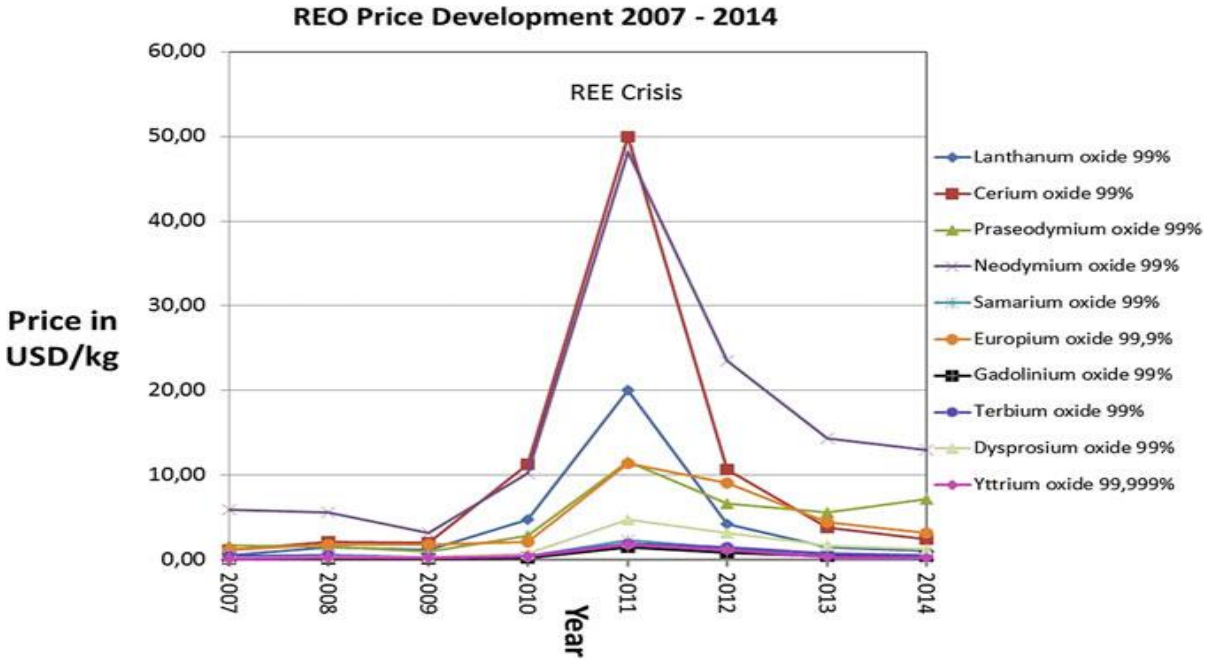

Figure 6: REO price development 2007–2014 (Voncken, 2016)

3. SEPARATION TECHNIQUES FOR REEs

3.1 SYNOPSIS OF CONVENTIONAL SEPARATION TECHNIQUES

REEs are extracted through complex chemical and physical treatment and often this process can cause hazards in the environment if not maintained under severe control. The tailings from these processes are major threats to human health. These tailings contain heavy metals and radioactive species which can cause severe damages to the environment. However, new technologies are attempting to decrease the contamination and provide safer environmental solutions. The typical extraction process can be modified based on factors like ore type, nature of compounds in the mineral, composition of REEs in mineral and the environmental safety of the process (U.S. EPA, 2012).

The first step in REEs mineral processing is unit operations followed by an enhancement in the concentration of REOs by employing acids and base solutions. Furthermore, the concentrate is subjected to different metallurgical operations i.e. solvent extraction, ion exchange, adsorption, electrochemical refining and supercritical extraction, selective oxidation and reduction, fractional crystallisation and precipitation, to separate REEs (voncken, 2016).

Different minerals go through different physical beneficiation introduced in the beginning of the process. It does not involve any chemical treatment but physical treatment has a severe effect on the REEs recovery in concentrate (Gupta and Krishnamurthy, 2005). These physical treatments include grinding, crushing and then collecting the ore by flotation, magnetic or gravimetric separation. These separated particles are converted into liquid concentrates after acid/alkali treatments and further metallurgical processes recover the REOs (U.S. EPA, 2012).

The figure below illustrates a general block diagram of the REEs extraction process.

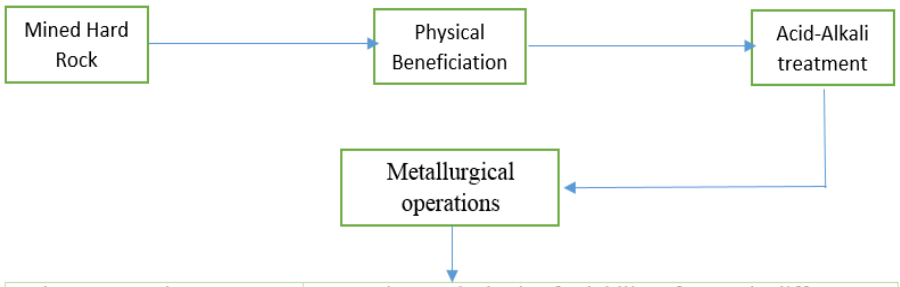

Solvent Extraction	Separation on the basis of solubility of REOs in different solvents
Ion exchange	Separation on the basis of their affinity towards ion exchange resin.
Adsorption	Physical or chemical deposition on solid surface
Electro winning	Extraction by electric current trough metal ion solution through electroplating
Electro refining	Anode made of REEs mixed(recycled) material; passing current release REEs from anode and deposited to cathode
Super critical extraction	Reaction with CO2 in Critical temperature and pressure which creates minute difference for separation
Selective oxidation/reduction	Oxidizing or reducing certain REE with different agents at different conditions and the extraction with solvents etc.
Fractional crystallization/ precipitation	Fractional crystallization by change in parameters to precipitate certain REE and precipitation by adding certain chemicals to precipitate any REE.

Figure 7: Extraction process layout for REEs (Adapted from U.S. EPA 2012; Voncker 2016; Gupta and Krishnamurthy 2005)

REEs removal from mineral ores of monazite or bastnasite is achieved typically by dissolving at high temperatures to base or acid solutions. Exposing minerals to these strong solutions in the presence of severe temperature conditions, convert most of the REEs to their hydroxide, chlorides or sulfates. After cooling these mixtures, thorium is removed by filtration, dissolution and selective precipitation. Xenotime also goes through a similar process where after treatment with sulfuric acid, phosphate is removed with water by leaching. After that, the selective precipitation of thorium and REEs sulfates is accomplished (Castor and Hedrick, 2006).

At Mountain Pass (California), bastnasite is subjected to calcination to remove gasses effluent i.e. CO_2 and F_2. Further treatment is done with HCl to digest all the REEs present and oxidising to yield CeO_2 residue. In Baotou (China), Bayan obo the mineral ore is treated with sulfuric acid to elevated temperatures of 300-600 °C. This converts REEs to sulfates which are leached out by water and recovered by precipitation as double sulfates. These doubles sulfate then are converted to hydroxides and leached out with HCl for purification by solvent extraction and other techniques (Castor and Hedrick, 2006).

Selective fractionation of REEs has been one of the greatest problems in chemistry because of their similarity in properties. Resultantly, it makes separation incredibly difficult. However, the key to separate REEs lies in their atomic radius which causes a slight change in their basicity. That slight difference affects the formation of complexes and their solubility in different solutes (Moeller 1945).

The separation techniques of fractional crystallisation and ion exchange, along with others, represent a small portion of existing methods for REEs removal. Most of the commercially employed methods are solvent extraction in liquid to the liquid phase. The process of solvent extraction is based on a series of steps where organic solvents are introduced in every step to fractionate different end products over each step. These end products go through mixing and settling units on every step. After precipitation and final drying, the end product yield is approximately 99.99% pure (Castor and Hedrick, 2006).

3.2 ADSORPTION METHODS FOR REEs REMOVAL

Until the 1950s, the methods of fractional crystallisation and precipitation were the only processes to separate REEs. These methods provided inefficient separation to the purity of 99.99 3N with larger residence times. However, from 1950 onwards, Ion exchange and

solvent extraction ruled the separation applications for REEs. Uses of these methods are limited to a smaller capacity but the higher purity of 99.99 7N can be achieved. Therefore, the target market focuses the high purity applications i.e. electronics etc. (Xie et al. 2014; Zhang et al., 2016)

These extraction methods are limited in several perspectives. The methods of fractionation are energy inefficient and consume higher time. Solvent extraction is limited to run small capacities and utilise huge amounts of organic solvents which yield higher amounts of environmental waste. Moreover, the process can be time consuming and might need hundreds of stages to achieve certain purity (Svard 2015). Hence, newer techniques are emerging to separate REEs in a much more effective and economical way. Among these methods, adsorptions are a sustainable, effective and environmentally friendly method. Its simple nature with higher removal efficiencies in a very low residence time make it very attractive for the REEs industry (Das 2013).

In the past few years, adsorption has gained much attention because of its simplicity and sustainability with great removal efficiencies in low residence time, compact size, ease of operation and environmentally friendly nature make adsorption and attractive option for commercial applications (Das and Das, 2013).

Globally there is a developing trend to utilise biodegradable organic matter for REEs adsorption (Butnariu et al., 2015). Biosorption is considered a potential source for recovering REEs from solutions (Cadogan et al., 2014). Furthermore, adsorption has been proved as an effective method to recover even very small concentrations of REEs from liquid solutions (Galhoum et al., 2015).

A literature survey reveals that there are dozens of novel publications which employed the idea of adsorption over different adsorbents. These include uses of naturally occurring biomaterials i.e. malt spent roots, chitosan, cellulose and other adsorbents as carbon nanotubes, modified silica, bypass cement and hydrogels etc. However, due to the huge amount of data, some publications from the year 2010 onwards are presented below.

Dubey and Rao (2010) synthesised hydrous ferric oxide for uptake of Ce (+3) from aqueous solutions at an adsorptive concentration (10^{-4}–10^{-8}) mol/dm^3. Ce ions attached chemically with the adsorbent surface and the process was favoured by an increase in the

temperature and pH of the solution. Reported adsorption followed Freundlich and D–R isotherm with maximum adsorption capacity of 5.63×10^{2} mol/g.

Adsorption of yttrium (Y^{3+}), neodymium (Nd^{3+}), gadolinium (Gd^{3+}), samarium (Sm^{3+}) and lutetium (Lu^{3+}) were reported over by-pass cement dust (BCD). BCD; is a by-product of Portland cement process, represents low-cost adsorbent which can effectively be used to remove precious metals. Sorption followed Freundlich isotherm and pseudo-second-order kinetics. Increase in temperature increased adsorption and maximum adsorption capacities reported at pH 7 were: 8.32 mg/g, 4.44 mg/g, and 5.87 mg/g, respectively, for Sm (3+), Nd (3+) and Gd (3+), respectively (Ali et al., 2011).

Eu (3+), one of the critical REE, was reported to be extracted by malt spent roots (MSR). MSR is unattractive low-cost commercial by-product of malting process. Adsorption behaviour of MSR and activated carbon was reported for a comparison. It was found that adsorption followed the Langmuir model and achieved equilibrium in 60 min. The maximum adsorption capacity reported was 152 mg/g for MSR and 88 mg/g for activated carbon. Considerable high value of capacity estimated MSR as good biosorbent for Eu (Anagnostopoulos et al., 2012)

Granados-Correa et al., (2013) reported hydroxyapatite as a low-cost effective adsorbent for La(3+) and Eu(3+). Hydroxyapatite $Ca_{10}(PO_4)_6(OH)_2$, was found out to be a useful material for the environment because of its adsorbing affinity for metals from wastes. Adsorption phenomenon was observed as a multilayer cooperative-type process and endothermic nature with pseudo-second-order kinetics and Freundlich adsorption isotherm. Reported adsorption capacities were 0.25 mg/g and 0.94 mg/g for La (3+) and Eu (3+), respectively.

Bio-sorption of Europium (+3) was reported by chitosan nanoparticles and carb shell particles from industrial and radioactive waste water. Adsorption was reported in a batch process with equilibrium time of 60 minutes and pseudo second-order kinetics represented by Langmuir isothermal model. Reported maximum adsorption capacity for chitosan nanoparticles and crab shell powder was 114 and 3.2 mg/g, respectively. Furthermore, adsorbent particles were characterised and reported by DLS, FTIR, TGA, XRD and SEM (Cadogan et al., 2014)

CemGok (2014) reported neodymium (3+) and samarium (3+) recovery by magnetic nano-hydroxyapatite. MNHA was reported as a good adsorbent with low cost and higher efficiencies. The adsorption reaches equilibrium in 150 min at an optimum pH 5.5. The data were fitted to pseudo second-order kinetics with Langmuir isotherm. The maximum adsorption capacity reported for Nd and Sm were 323 and 370 mg/g, respectively.

Roosen and Binnemans (2014) modified chitosan with EDTA and DTPA, for the uptake of REEs from batch solutions. The modified chitosan biopolymer was reported to selectively extract REEs from solutions with slight changes in pH. Reported maximum adsorption capacity for Nd(+3) was found out to be 74 mg/g for EDTA-chitosan and 77 mg/g for DTPA-chitosan.

Wang et al., (2014) synthesised calcium alginate-poly glutamic acid hybrid gel by cross-linking PGA on Ca-ALG. PGA was reported to enhance the adoption properties of alginate effectively and increase the adsorption capacity from 1.35 to 1.65 mmol g^{-1}. Adsorption data were fitted best with Langmuir and pseudo second-order kinetics. Reported adsorption was an increasing function of atomic number from La to Pr while an opposite trend from Sm to Lu. Y represented minimum adsorption capacity and Sc with highest.

Carbon nanoparticles were reported to remove La(+3) and Nd(+3) from aqueous solutions, in work presented by Younis et al., (2014). The optimum conditions of adsorption were found to be 0.02g of CNPs per 25ml of wastewater at pH 7. Adsorption reaches in 40 min with maximum adsorption capacity of 0.51 mg/g.

Butnariu et al., (2015), reported uptake of REEs using bone powder, a naturally occurring biodegradable organic adsorbent. Adsorption was reported in a batch process with equilibrium time 60 min. Experimental data was found to fit best with Langmuir isotherm with a maximum capacity of 10.75, 12.6 and 8.43 mg/g for Nd (+3), Eu (+3) and La (+3), respectively. Furthermore, results showed a comparative adsorption of +1 and +2 ions had fewer tendencies towards bone powder than +3 REEs.

Chitosan embedded with magnetic nanoparticles and modified with Cysteine ($C_3H_7NO_2S$), was reported to uptake La (+3), Nd (+3) and Yb (+3) from batch solutions. Adsorption reached equilibrium in 4h following pseudo second-order kinetics. The pH of 5 was stated to be optimum yielding maximum adsorption capacities of 17.0, 17.1 and 18.4 $mg \cdot g^{-1}$ for La (+3), Nd (+3) and Yb (+3), respectively. Moreover, the adsorption process showed

spontaneous endothermic nature and the data was fitted successfully with Langmuir isotherm (Galhoum et al., 2015).

Khotimchenko et al., (2015) stated the removal of Y (+3) from batch solutions by calcium and sodium alginate. Adsorption achieved equilibrium in 60 min following pseudo second-order kinetics. Additionally, experimental data showed good fit by Langmuir isotherm with maximum adsorption capacities of 99.01 and 181.81 mg/g for calcium and sodium alginates, respectively, at pH 6.

Silica-formaldehyde composite combined with 2-ethylhexylphosphonic acid mono-2-ethylhexylester was reported to uptake Eu (+3) and Nd (+3) form aqueous solutions. The process of adsorption was controlled by the intra-particle diffusion model with pseudo second-order kinetics. Maximum adsorption capacities for Eu (+3) and Nd (+3) were reported 3.1 and 2.8 mg/g, respectively (Naser et al., 2015).

Granular hybrid gel, formed by acrylic acid with hydroxylpropyl cellulose and fabricated with attapulgite as inorganic constitute, were reported for uptake of La (3+) and Ce (3+) from aqueous solutions. Adsorption process, for pH over 4, followed pseudo second-order kinetics with Langmuir isotherm. Equilibrium was achieved in 40 minutes and the maximum adsorption capacities were 270 and 200 mg/g for La(3+) and Ce(3+), respectively (Zhu et al., 2015).

EDTA-β-cyclodextrin was reported for uptake of La (+3), Ce (+3) and Eu (+3), from batch cycles. EDTA-β-cyclodextrin, a bio-sorbent, bonded REEs chemically following pseudo second-order kinetics and Langmuir isotherm. Reported maximum capacities were 0.343, 0.353 and 0.365 mmol/g for La (+3), Ce (+3) and Eu (+3), respectively (Zhao et al., 2016).

Yao et al., (2016) described the adsorption of Eu (+3) on sulfonated graphene oxide (GO-OSO_3H). Graphene oxide was grafted by the highly acidic environment of concentrated H_2SO_4 to form the composite. Adsorption followed pseudo-second-order kinetics with Langmuir isotherm. Moreover, thermodynamics suggested the process was exothermic in nature hence favoured by a decrease in temperature. Maximum adsorption capacity was found out to be 125.0 mg/g at pH 5.5.

Carbon nanoshells, synthesised from carbonisation of polydopamine, were reported for the enrichment of REEs in solution. These carbon shells were reported to be better adsorbents

than solid carbon spheres. Their affinity was stated to be more towards LREEs and lesser to the middle (i.e. Gd+3) and HREEs (Xiaoqi et al., 2016).

Iftekhar et al., (2016) reported Zn/Al LDH intercalated cellulose nan-ocomposite, for uptake of Y (+3), La (+3) and Ce (3+), from batch solutions. Adsorption equilibrium was achieved quickly, in 10 minutes, following pseudo second-order kinetics. Experimental data were fitted to Langmuir model yielding maximum adsorption capacities of 102.25, 92.51 and 96.25 mg/g for Y (+3), La (+3) and Ce (3+), respectively. Furthermore, the authors also reported the removal of Eu (+3), La (+3) and Sc (3+), by cellulose-silica nanocomposite in 2017. The kinetics were controlled by film diffusion, also, Eu (+3) and La (+3) were stated to chemically attach, while, Sc (+3) was reported to physically adsorb, on the surface of adsorbent. Moreover, adsorption behaviours of Eu (+3) and La (+3) were modelled to Langmuir isotherm, while, Sc (+3) fitted best to Freundlich. Maximum adsorption capacities were reported 24.47, 29.48, 93.54 mg/g for Eu (+3), La (+3) and Sc (3+), respectively.

Modified mesoporous and microporous silica gels, with PAN and Acac, functionalised with amines; 3-aminopropyl triethoxysilane (APTES) and 3-aminopropyl trimethoxysilane (APTMS), and with non-amines; trimethoxymethylsilane (MTM) and chlorotrimethylsilane (TMCS), were reported to uptake REEs from aqueous batch solutions. A comparative study was represented to illustrate the best modification for silica surface chemistry. Results represented the mesoporous silica gel of particle size of 15–20 μm, functionalised with APTES and APTMS, showed the best uptake of REEs. Furthermore, the modification of silica by PAN and Acac, with and without APTES and ATPMS, showed that PAN modified gels were the most impressive for REEs extraction. PAN showed almost complete adsorption in 5 hours for all REEs (≤50 ppm) under study. Furthermore, pH greater than 7 was stated to be feasible for physio sorption by PAN/Acac modified silica, whereas, amino-modified silica showed greater adsorption in acidic medium. A cost estimate suggested €900-1,200, for treatment of $1m^3$ of waste water by 1 kg of adsorbent (Ramasamy et al., 2017).

4. LAYERED DOUBLE HYDROXIDE

4.1 INTRODUCTION, PROPERTIES AND APPLICATIONS

LDH, often referred to as anionic clays, are two-dimensional solids containing positively charged brucite layers of mixed metal oxides (Nakawade et al., 2009). LDHs formation occurs when divalent ions are replaced with trivalent ions and, therefore, the positive charge is compensated by introducing anions to the double layers (Iftekhar et al., 2016). Hence, incorporating different anions makes LDHs as multifunctional chemicals with applications in separation, catalysis, medical field and Nano-Engineering technology (Nakawade et al., 2009). LDHs are represented by the following general formula:

$$[M^{+2}_{1-x}M^{+3}_{x}(OH)_2]^{x+}[A^{n-}]_{x/n}.mH_2O$$

In above equation M (+2) and M(+3) are the di and trivalent cations, respectively, the A^{n-} is replaceable anion; and 'x' is the ratio of $M^{+3}/(M^{+2}+M^{+3})$ which determines the charge density of the layers (Dan et al. 2016). Furthermore, the amount of anionic species required to balance the positive charge can be determined from stoichiometry with the known M^{+3}/M^{+2}ratio (Theiss et al., 2016).

The mixed metal ions are connected with hydroxyl ions, positioned on an octahedron, to form bi-dimensional sheets similar to brucite($Mg(OH)_2$) sheets. Approximately one fourth to half of the divalent ions are replaced with trivalent ions to give a net positive charge to the sheets (Theiss et al., 2016). These positively charged sheets are stacked together intercalated with anions to form a bi-dimensional LDH composite material (Iftekhar et al., 2016). Organic-inorganic composites with LDHs, depending on the type of anion, LDHs can be functionalised for specific applications (Kameda et al. 2006).

One of the distinct properties of LDHs is the absence of cross-linking between the layers. This allows the layers to expand or contract to fit in different types of anions. Hence, due to that, LDHs are easily tailored for the desired functions and can be applicable in vast applications (Theiss et al., 2016). Another interesting feature of LDHs is the reconstruction of LDHs after calcination called the 'Memory Effect'; in which an LDH molecule recover its initial state after once destroyed by heat. However, it was noticed that this reconstruction is highly dependent on the calcination conditions i.e. a partial reconstruction

in case of higher temperatures and total loss of Memory effect in case of even severe conditions (Li and Duan, 2005).

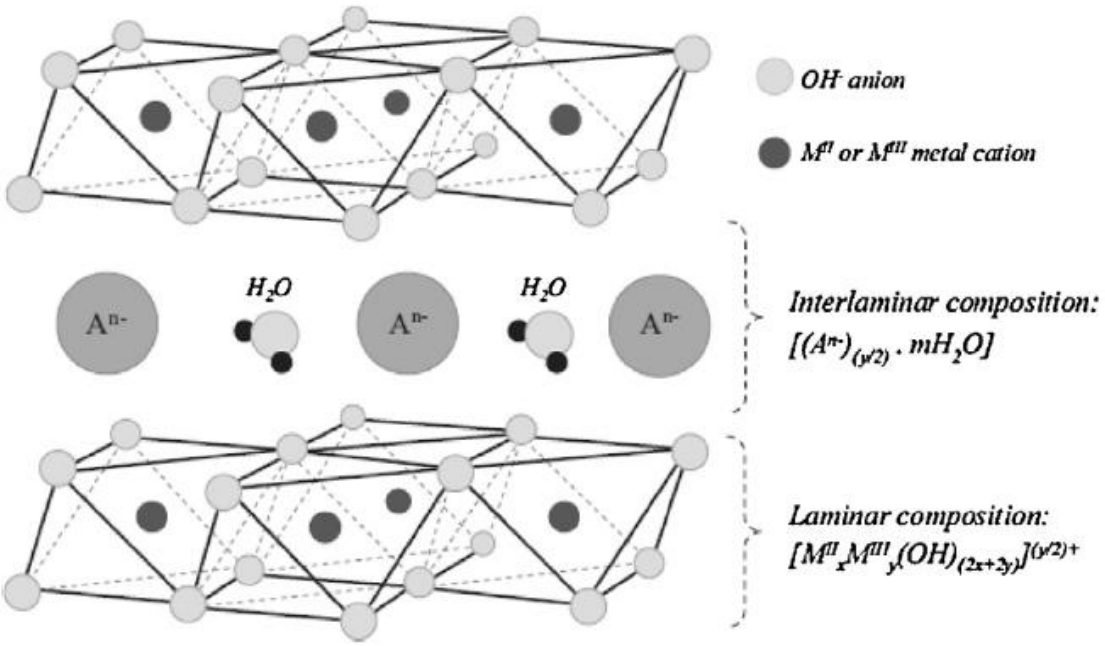

Figure 8: Structure of LDH (thesis et al., 2016)

The flexible and versatile nature of LDH to incorporate with different materials makes it adaptive for enormous applications. Some potential uses include as biochemical drug i.e. anticancer drug for cancer therapy, improving the stability of vitamins, bio-hybrid gene carrier to target certain organs and cells. As a catalyst, i.e. Ni/Al LDH for hydroxylation of phenol, carboxylation of methanol, natural gas conversion, as adsorbent i.e. uptake of metals form solutions, for phenol removal, fluorine removal from aqueous media, cationic and anionic dyes remover, in electrochemistry i.e. as cheap and stable electrodes, as composite electrolytes to enhance conduction and other properties etc.(Li and Duan, 2005).

4.2 LDH AS AN ADSORBENT

A recent advance in adsorption techniques reveals that there have been several LDH materials which are used to uptake both anions and cations. These multifunctional LDH can extractions from solutions through; surface adsorption, interlayer ion exchange and reconstruction of destroyed LDH through calcination by the Memory effect (Li and Duan, 2005).

From a literature survey, it was revealed that LDHs have been employed for enormous applications and several authors reported their use as an adsorbent. A summary of some of this noble work is presented in the table below:

Table 4: LDH based adsorbents

Adsorbent	**Adsorbate**	**Adsorption conditions/ Results**	**Reference**
Mg-Al LDH with 2-naphthalene and 2, 6-naphthalene disulphonate	bisphenol	Al/Mg mole ratio 1/3, adapted pH 10.	Kameda et al., (2006)
Mg-Fe-CO_3 LDH	La (+3) and Nd (+3)	120 min contact time, adsorbent dose 0.1 g/ 10 ml at pH 1, maximum adsorption capacity 480 mg/g for La and 192 mg/g for Nd, regeneration by 2M HCl.	Gasser and Aly (2013)
Mg-Al-Cl LDH with doping of Fe^{2+}	Se (VI)	Fe^{2+} doping enhances over all adsorption as part of Se (VI) is removed by ion exchange with intercalated Cl^{-1} while a part of Se (VI) is removed by reduction of Se (VI) to Se (IV) by the oxidation of Fe^{2+} to Fe^{3+}, maximum adsorption capacities 1.4 $mmol^{-1}$ g^{-1}.	Kameda et al., (2014)
Mg-Al-CO_3^- LDH and magnetic Fe_3O_4/ Mg-Al-CO_3^- LDH	Cd(II)	Maximum adsorption capacities 70 mg/g and 55 mg/g, respectively, for Mg-Al-CO_3^- LDH and magnetic Fe_3O_4/ Mg-Al-CO_3^- LDH.	Shan et al., (2015)
Mg-Al LDH from slow pyrolysis of bagasse biomass	antibiotic tetracycline	Maximums adsorption capacity of 1118.12 mg/g.	Tan et al., (2016)

4.3 GUM ARABIC MODIFIED PARTICLES AND APPLICATIONS

G.A. is a well-known food additive and is often employed as rheology and viscosity modifier in the food industry. Due to the non-toxicity and unique properties of G.A. it has been widely used in the food sector for decades (Osman et al., 1993).

Recent advances in research show that authors like Banerjee and Chen (2007), Srivastava et al., (2015) Barik et al., (2015) and Ribeiro et al., (2014) have found applications of G.A. for sectors other than the food sector. In this noble work, G.A. is modified in several ways to obtain the desired features and applications. A summary of their work is presented in the text below.

Banerjee and Chen (2007) utilised a co-precipitation method to fabricate magnetic nanoparticles in G.A. via interacting surface hydroxyl groups of magnetic oxide and carboxyl groups of gum. Characterisation results suggest that there was no phase modification of magnetic particles while a surface modification was realised. The nanoparticles produced uptake copper ions in aqueous media in a rapid manner and equilibrium was established within 2 min. Adsorptions capacities reported were 38.5 mg/g following Langmuir fitting and adsorption constant of 0.012 L/mg.

Srivastava et al., (2015) produced MgO nanoflower by chemical precipitation along with G.A. These nanoparticles were characterised with XRD, TEM, SEM and AFM; which confirmed a coating of G.A. was achieved during this green synthesis of MgO nanoflower. Furthermore, these modified MgO nanoparticles were utilised for uptake of divalent cationic ions i.e. copper, cadmium, zinc, cobalt etc.

Barik et al., (2015) presented a characteristic and electrical study of G.A./ZnO nanocomposite. Nanoparticles were obtained by the co-precipitation method and were confirmed by TEM in the nano range of ~40nm. Furthermore, the nanocomposite was evaluated for electrical applications i.e. dielectric in high frequency applications.

Ribeiro et al., (2014) prepared modified G.A. by utilising sodium trimetaphosphate as a cross-linking agent. This modification was studied for variations in physical and chemical properties by changing cross-linking agent concentrations. In addition, citrates oil encapsulation efficiency was tested for modified conditions of synthesis. The results

suggest that cross-linking with 6% sodium trimetaphosphate provided the best encapsulation efficiency with desired rheology and swelling characteristics.

4.4 GENERAL METHODS OF PREPARATION OF LDH

In the literature review herein above it has been revealed that LDH has been synthesised in multiple ways and utilised in many applications i.e. adsorption, water treatment and drug delivery etc. The co-precipitation method is the most common method employed to produce LDH either in one step or introducing an ageing step later after precipitation. Other methods include ion exchange, reconstruction of LDH or 'Memory effect', hydrothermal and other miscellaneous methods.

The co-precipitation method is one of the most wildly employed methods to synthesise LDH in one step. Due to the simplicity and direct approach, commercial LDH are preferably prepared by co-precipitation. In this preparation technique, a mixed metal solution of M (+2)/ M (+3) is prepared on a desired ratio and is used as precursor in aqueous media containing soluble anionic specie. The precursor ions can be of same metals or mixed metals depending on the choice of synthesis. Flexibility in metals choice and the ratio used in synthesis creates a difference in layer charge density and hence a wide range of LDH of same constituents can be formed. This produces a wide range of alternatives which can be compared for functional properties and chosen to serve for the best results.

To ensure the simultaneous co-precipitation of species, it is necessary to provide strict pH control during LDH synthesis. The choice of pH is often dependent on the ions incorporated and the type of LDH made. In some cases, LDH might need supersaturation conditions to precipitate simultaneously divalent and trivalent ions and hence formulate the LDH structure. This supersaturation is often achieved by pH control and hence providing a higher or equal pH level required to precipitate most soluble metal hydroxide under consideration (He et al., 2005).

Metal chlorides or nitrates of mixed or multiple metals are preferably used to ensure LDH structure as the metal ions incorporation with desired anionic species can be differed in the presence of more attractive anions. Moreover, introducing metal chlorides often make synthesis conditions achievable even on low saturation degrees. The degree of intercalation hence is not dependent on competing ions and is more of a function of pH levels, the ionic charge of brucite layers and anion concentration.

Co-precipitation, as explained herein above, is achieved by introducing basic media to attain a certain level of pH for precipitation. Some species i.e. urea, can accomplish the same synthesis without a need of external base. The process is often named as; urea hydrolysis, where urea undergoes hydrolysis in two steps. First, where the urea molecule is converted slowly into ammonium cyanate; which determines the rate of reaction. Second, where cyanate is converted into ammonium hydroxide base and carbonate ion. The presence of ammonium ion creates a shift in pH levels to basic media which cause co-precipitation and LDH formation. Due to the self-sustainability of the method, it is often employed to precipitate metals LDH precipitates. Reaction equation below illustrates urea hydrolysis and the production of ammonium base in water:

$$CO(NH_2)_2 \rightarrow NH_4CNO$$
$$NH_4CNO + 2H_2O \rightarrow 2NH_4 + CO_3^{2-} \quad (1)$$

A similar hydrolysis has been reported by Costantino et al., (1998); they were able to analysis multiple divalent ions i.e. Ni (+2), Mg (+2) etc, with trivalent Al (+3). The report represents an investigation of LDH prepared by varying metal concentration, urea molar fraction and urea to metal ion ratio to get better LDH crystals. The results suggest a 3.3 molar ratio of metal ions to urea where the divalent to trivalent ratio of 0.33 in 0.5 M solution of urea yields the best LDH crystals. Furthermore, experiments proved that Mg/Al LDH was not easily obtainable at low charge densities, so the urea method can be utilised to obtain high charge density Mg/Al LDH particles.

Several physical treatments are often introduced followed by co-precipitation i.e. ageing, thermal treatment, hydrothermal treatment etc. Depending on the treatment employed, characteristics of LDH particles obtained can be modified i.e. improving crystalline structure, increment in amorphous structure or changing particle size distribution etc.

In some cases, an ion exchange method is considered more preferable than co-precipitation i.e. if the metal ions are not stable in basic media or a direct reaction between the anionic specie is more favourable than co-precipitation. Hence, in ion exchange, a simple approach of exchanging ions over already prepared LDH is performed which produces the required LDH in a one step synthesis (equation below).

$$LDH \cdot A^{m-} + X^{n-} \rightarrow LDH \cdot (X^{n-})m/n + A^{m-} \quad (2)$$

$$LDH \cdot A^{m-} + X^{n-} + mH^{+} \rightarrow LDH \cdot (X^{n-})m/n + H_m \quad (3)$$

These ions exchangeable LDH normally contain less attractive and more stable anionic specie i.e. chlorides etc. Therefore, in favourable conditions other anions i.e. carbonates etc., which are more attractive towards LDH sheets, can be replaced with those chlorides forming desired LDH.

However, the ion exchange method is highly controlled by the electrostatic forces between the host and exchangeable ion. The governing mechanism of exchange is an attractive force which causes a shift in ions over target LDH surface. The order of affinity hence follows the standard potential of anionic and cationic species for their capability to replace an ion on LDH surface. Exchanging media also plays vital role in ion exchange i.e. organic media facilitates organic ions substitution on LDH while aqueous media assist inorganic ions replacement. Controlling pH is essential for achieving a certain level of substitution and the charge density of LDH host can be controlling factor for incoming species.

An interesting feature of LDH is their regeneration from a calcined LDH. Calcination of LDH destroys the LDH structure as the removal of hydroxyl groups, anions and water of hydration, which leaves mixed metal oxides. These mixed metal oxides can be reconstructed in water by using any anionic specie which can be other than the one used before calcination. The memory effect is often utilised to incorporate large and complex ions into LDH structure as it makes the intercalation easier due to no competing anions as in other synthesis methods (He et al., 2005).Hence, any desired LDH can be generated through the memory effect i.e. common examples include the generation of several herbicides, surfactants, dyes etc.

Hydrothermal methods are often referred to prepare LDH with species which are less attractive towards LDH. Introducing divalent and trivalent hydroxides as LDH hosts leaves other competitive ions except hydroxides which are very less likely to compete with base due to low affinity. Renaudin et al., (1999) reported such hydrothermal method to prepare Ca/Al LDH with calcium carbonate. Results showed that the structure of obtained LDH can be modified by employing a temperature change during the process as it affects the ordering and stacking of LDH layers.

5. ADSORPTION THEORY AND MODELLING FRAMEWORK

5.1 ADSORPTION THEORY

The phenomenon of absorption occurs when a driving force causes certain chemicals to shift phases and get attached to the surface of the adsorbent. Adsorption is happening mainly on the surface where the particles from liquid or gas get attracted to the adsorbent surface due to Vanderwall attractions or stronger chemical bonds. This propagation of adsorbate from bulk to adsorbent occurs when the driving force or attractive force is higher to that cohesive force keeping the molecule in bulk (C.T. Chiou, 2001).

The adsorption system under this research includes a solid surface of Mg-Al-G.A. LDH tested for six different REEs in aqueous solution. Adsorption occurs when REEs from liquid media get attached to LDH surface which can be observed by measuring their concentration in solution after adsorption. This adsorption of REEs is limited to adsorption equilibrium which is achieved after a certain amount of time. The equilibrium point established shows maximum adsorption possible in provided conditions of time, concentration, pH, temperature and adsorbent dose.

Adsorption can be classified on the basis of interaction of adsorbent and adsorbate i.e. permanent or virtual non-permanent. If adsorption happens permanently and the adsorbate species cannot be removed without a chemical aid, adsorption is referred to as chemisorption. Chemisorption hence yields a high amount of enthalpy change i.e. > 50 kJ/mol due to the creation of metallic bonds with the adsorbent. In another case, where adsorption happens physically mainly due to Vanderwall attractions and does not cause enthalpy changes higher than 50 kJ/mol is referred to as physisorption. Hence, physisorption can be reversed by just employing heat and without a chemical aid while chemisorption acquires chemical aids to replace the adsorbed metal from the surface.

The relationship between adsorbent and adsorbate is described as a function of adsorbent dose, adsorbate concentration, pH value, temperature and contact time. In the given conditions, if all other factors are kept constant then graphical trend between capacity and time is known as adsorption isotherm (equation 4). These factors also determine the rate at which any adsorbate is removed from bulk i.e. providing higher temperature can improve adsorption rates if the relationship between adsorbate and adsorbent is endothermic. In

addition, a change in pH can decrease or increase attractive forces by affecting interactions between adsorbent surface and adsorbing species.

$$q_e = q\ [C_e(equilibrium\ concentration), t(time)] \quad (4)$$

5.2 MODELLING FRAMEWORK

5.2.1 ADSORPTION ISOTHERMS

An adsorption isotherm illustrates a relationship between the adsorbate and adsorbent surface graphically. At a fixed temperature, concentration, adsorbent dose, pH and equilibrium time; illustration of adsorption capacity and time represent adsorption isotherm. Adsorption isotherms can reveal if adsorption is suitable in lower or higher concentration of solute. Similarly, the maximum amount of adsorbate which can be removed through an adsorption cycle, often called adsorption capacity, is also determined through isotherms.

In any adsorption isotherm, adsorbent and adsorbing species are kept in contact until a dynamic equilibrium is achieved between solid and bulk. The dynamic equilibrium limits the maximum adsorption possible in certain temperature and pH conditions. In general, an adsorption phenomenon can represent any of the following isotherms according to Brunauer, Emmett and Teller or shortly BET (Figure 9).

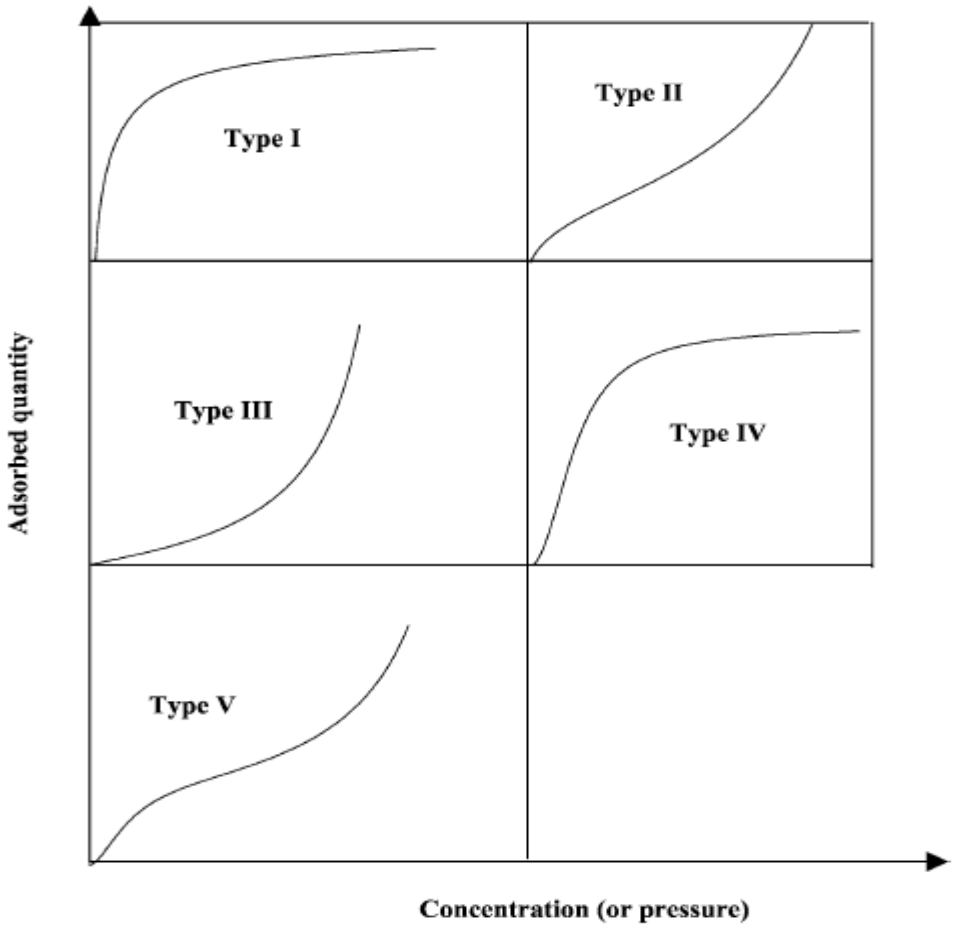

Figure 9: Types of adsorption isotherms according to BET Modelling (Khalfaoui et al., 2003)

Several mathematical methods are present to model the experimental results. In the present work, three models, namely **Langmuir, Freundlich** and **Temkin** isotherms, have been used to analyse the experimental results. A brief introduction to these models is presented in the text below.

5.2.2 LANGMUIR ISOTHERM

Langmuir modelled this adsorption isotherm in 1916. He studied the adsorption of gas vapours on solid surfaces with fixed and identical adsorbing sites. This model firstly was used to develop mathematically adsorption behaviour of gases on the solid activated carbon surface. Carbon surface was assumed to have fixed and same receptor sites which could be filled only with one molecules layer representing monolayer adsorption throughout. Langmuir also considered the interacting molecules have no hindrance and they do not show competitive behaviour for an adsorption site.

Considering all the factors alongside the modelling equation can be represented as follows:

$$q_e = \frac{q_m K_L C_e}{1+K_L C_e} \quad (5)$$

The linear form which can be expressed as:

$$\frac{Ce}{qe} = \frac{1}{K_L q_m} + \frac{Ce}{q_m} \quad (6)$$

Langmuir model has been employed in several research studies to predict the adsorption behaviour. The model can predict maximum adsorption capacity and Langmuir constant K_L, which can predict favourability of adsorption by expression below:

$$R_L = \frac{1}{1+K_L C_e} \quad (7)$$

Adsorption is considered unfavourable if $R_L > 1$, favourable if $0 < R_L < 1$, linear if $R_L = 1$ and irreversible if $R_L = 0$.

5.2.3 FREUNDLICH ISOTHERM

Herbert Freundlich modelled this earliest known isotherm in 1906. This model considered more realistic approach towards interaction between receptor sites and molecules being non-ideal i.e. non-monolayer, reversible and heterogeneous adsorption. Freundlich used animal charcoal to study adsorption and estimated a logarithmic decrease in adsorption energy when an adsorption site was filled.

The mathematical expression of this model is described as follows:

$$q_e = K_f C_e^{1/n} \quad (8)$$

The linear form of which can be expressed as:

$$\ln qe = lnK_f + \frac{1}{n}\ln Ce \quad (9)$$

The slope of the model can predict adsorption nature i.e. slope value closer to zero indicate an increase in heterogeneity and closer to 1 indicates the chemical interaction of molecules with an adsorbent (Foo and Hameed, 2009).

Even though the Freundlich model has been used to estimate heterogeneous adsorption on a solid surface it is noted that the model does not reduce to Henry's law at lower concentrations. Hence, other fitting models with a better theoretical basis are often taken into account.

5.2.4 TEMKIN ISOTHERM

Mikhail Temkin made this model through empirical relationships in 1941. Temkin generated this adsorption model while studying hydrogen adsorption on platinum electrodes. The model assumes that, unlike the Langmuir model, the adsorption surface can be heterogeneous also. The logarithmic decrease proposed by Freundlich was considered linear by Temkin. He estimated adsorption by ignoring extremely low and high concentration, where the adsorbing molecules tend to have uniform binding energy distribution.

An empirical equation of this model is as follows:

$$q_e = \frac{RT}{b_T}\ln(A_T C_e) \tag{10}$$

The linear form of which can be expressed as:

$$q_e = \frac{RT}{b_T}\ln(A_T) + \frac{RT}{b_T}\ln(C_e) \tag{11}$$

5.2.5 ADSORPTION KINETICS

The kinetics of the adsorption phenomenon refers to mass transfer rates which control the residence time of adsorption. Form kinetics valuable information about the rate of adsorption is determined which determines the residence time and hence the design parameter i.e. adsorption vessel dimensions can then be determined.

Theoretically, any adsorbing particle passes through 4 stages in adsorption phenomenon:

1. Mass transfer of adsorbate particle to a bulk solution
2. External diffusion: diffusion of molecules from the thin film formed by solution around the adsorbent particles. This mainly happens due to the presence of attractive forces

present between adsorbing molecules and adsorbent surface. This produces a diffusion gradient across the thin film.

3. Intra particle diffusion: this refers to the movement of the particle into the porous structure of solid adsorbent.

4. Adsorption of the molecule on the surface of adsorbent i.e. either chemically or physically depending on the adsorption enthalpies involved.

As the adsorption rates can be defined on any of the steps explained herein above, modelling adsorption kinetics can be either defined on the basis of diffusion or on the reaction. In every adsorption, a diffusion or adsorption reaction could define the total rate of adsorption. Diffusion models i.e. intra particle diffusion model, liquid film diffusion model etc, and non-diffusion model include pseudo first, pseudo-second order and Elovich model.

For the present study non-diffusion models; pseudo first order and pseudo second order are studied while diffusion models; Weber-Morris (also known as intra-particle diffusion) and Boyd diffusion, are investigated for adsorption kinetics. Brief introduction of these models with their modelling equations is given below.

5.2.6 ADSORPTION KINETICS BY REACTION MODELLING

If the reaction between the adsorbent and the adsorbing molecule is the slowest step, then it defines the rate of adsorption reaction. Reaction modelling can be done simply by defining a free site where an adsorbent molecule can get adsorbed to produce a filled site:

$$free\ site + adsorbate\ molecule \underset{k2}{\overset{k1}{\leftarrow\!\!\rightarrow}} filled\ site \tag{12}$$

Differential equation for the above reaction can be written as follows:

$$\frac{dq}{dt} = k_1\,(q_{max} - q)^n - k_2\,(q)^n \tag{13}$$

The model equation (13) can lead to a different interpretation as the value of ‘n’ in the equation determines the order of reaction.

Pseudo first order reaction rates, first determined by Lagergren in 1898, can be determined by considering ‘n=1’ in the above equation. Therefore, pseudo first-order rate equation at any particular time can be written as follows:

$$\frac{dq}{dt} = k_1 (q_e - q_t) \tag{14}$$

Converting above equation into linear form by integration:

$$log\ (q_e - q_t) = \log q_e - \frac{k_1}{2.303} t \tag{15}$$

Above equation can be converted to its non-linear form as follows:

$$q = q_e\ (1 - e^{-k_1\ t}) \tag{16}$$

Pseudo-second order reaction rates, first determined by Ho in 1995, can be obtained by replacing 'n=2' in equation (13). Second order kinetics shows two sites are involved for each adsorbate molecule which follows Langmuir type adsorption. Often these rates are determined by chemical reactions occurring on adsorption sites. Equation (13) can be reduced for this model:

$$\frac{dq}{dt} = k_1 (q_e - q_t)^2 \tag{17}$$

Converting the above equation into linear form yields:

$$\frac{t}{q_t} = \frac{1}{k_2 q_e^2} + \frac{1}{q_e} t \tag{18}$$

Above equation can be converted to its non-linear form as follows:

$$q = \frac{k_2 q_e^2 t}{1 + q_e k_2 t} \tag{19}$$

5.2.7 ADSORPTION KINETICS BY DIFFUSION MODELLING

Modelling kinetics by diffusion focuses the diffusion as the rate determining step. As observed in the above illustration, it can be concluded that the diffusion rate can control adsorption in two ways i.e. liquid film diffusion or intra particle diffusion. To estimate the diffusion mass transfer rate for liquid film diffusion, the Boyd equation is often used and, for estimating intra particle diffusion mass transfer, the Weber-Morris model can be applied.

The Boyd model can be mathematically described as:

$$\ln\left(1-\frac{q_t}{q_e}\right)=k_f t \tag{20}$$

The Webber-Morris diffusion model is expressed as:

$$q_t = k_i t^{1/2} + C \tag{21}$$

Linear plot of equation (21) determines that the diffusion mass transfer rate is only controlled by intra particle diffusion. On the other hand, if the Boyd fitting curve passes through origin the adsorption is controlled by intra-particle diffusion, else, it is defined by film diffusion.

5.2.8 THERMODYNAMIC MODELLING

Process of adsorption can be largely affected by the change in temperature depending on the type of adsorption phenomenon. In case of physical adsorption, an increase in temperature causes a weakening of Vanderwall forces which turns into the desorption of particles. In contrast, if the adsorption phenomenon is governed by chemical reactions, temperature dependence can be defined by the nature of reaction involved. Hence, an estimation of heat energies involved i.e. reaction enthalpy and Gibbs free energy, can determine the temperature effect on adsorption (Bartell et al., 1951).

Thermodynamic parameters, Gibbs free energy (ΔG^0), enthalpy (ΔH^0) and entropy (ΔS^0) can be related for adsorption as:

$$lnKc = \frac{\Delta S^\circ}{R} - \frac{\Delta H^\circ}{RT} \tag{22}$$

$$\Delta G^\circ = -RT \ln Kc \tag{23}$$

5.2.9 MODELLING ADSORPTION ISOTHERMS AND KINETICS

From the above equations, all the linear models are easily comparable to stranded linear form '$Y = mx + C$', by plotting the graph between 'Y' and 'X' in the equation, slope and intercept determines different constants. Moreover, the linear error function can determine the fit accuracy in model. Using non-linear model needs different approach where estimated values of constants are used to calculate parameter by minimising error function.

In the present study, an ‘R square’ error has been used which can be estimated from Microsoft excel 2017 by using linear trend line over the experimental data. The trend line equation can also be determined from the same graph by which estimation of different parameters can be done easily. For a better estimation, it is compulsory to have the ‘R square’ error close to unity.

To estimate the parameter from non-linear functions, Microsoft Excel solver function was used, which minimises the error of the given parameters by changing the values of constants. The results obtained were compared graphically and the errors were compared.

6. EXPERIMENTAL PART

6.1 GENERAL BASIS

All the experiments were conducted at the DGC lab located in Mikkeli. In experiments, 6 REEs, namely Sc, Y, Nd, Ce, Eu and La, were tested for adsorption from their aqueous solution in DI water on prepared Mg-Al-G.A. LDH. All the experiments were carried out in batch form. The weighing of adsorbents was done on a standard weigh machine Radwag AS 220/X. These batch tubes contained 50 ppm solution in 10 ml of respective REEs along with 10 mg dose of LDH adsorbent. The tubes were stirred in shaker IKA KS 4000 Control, for a specified time at room temperature and 200 rpm. After adsorption, the solution was filtered using a 0.45μm PTFE syringe filters.

ICP-OES (Agilent ICP-OES 5110) was used for testing the REEs concentration in solution after adsorption. ICP standards of metals under consideration were prepared in nitric acid solution using ICP standard metal solutions. These metals standards were run before to make a calibration curve, this curve was further used to the obtained concentration of experimental samples. A calibration curve was run again after one batch of reading was noted.

Adsorption experiments were carried out in the sequence of finding the best parameters for pH, dose etc. Firstly, the pH was adjusted and all the metal ions solution with fixed dose was run in different pH solutions. To adjust the pH of REEs solution 0.1 and 0.01 M NaOH and HCl solutions were used. The best pH found after the experiments were further

used to find the optimum dose. This optimum dose and pH values were adapted for further experiments of isotherms and kinetics.

Unless stated all the experiments were carried out at ambient temperature and pressure with a constant stirring speed of 200 RPM. All the samples were analysed by ICP and capacity and removal percent were calculated by the following formulas:

$$Removal\ \% = \frac{C_{initial} - C_{final}}{C_{initial}} \times 100 \quad (24)$$

$$q = \frac{(C_0 - C_e)V}{m} \quad (25)$$

Where, in the above equation, q is the adsorption capacity in mg/g, V is the volume of batch solution in litres, m is the mass of adsorbent used in grams, C_o and C_e are initial and equilibrium concentrations in parts per million.

Along with adsorption experiments, the characterisation was also performed to determine structural information of prepared LDH. This characterisation determined information of elements, size ranges on atomic levels, phase composition and particle size, microstructure and morphology of LDH sheets. The equipment used in characterisation includes FTIR, XRD, TEM, AFM and SEM.

6.2 MATERIALS AND METHODS

6.2.1 CHEMICALS

Chemicals used during course of present study include: G.A. from acacia tree, magnesium nitrate hexahydrate ($Mg(NO_3)_2 \cdot 6H2O$),aluminium nitratenonahydrate ($Al(NO_3)_3 \cdot 9H2O$), hydrochloric acid (HCl), sodium hydroxide (NaOH), yttrium chloride (YCl_3), cerium chloride heptahydrate ($CeCl_3 \cdot 7H_2O$), lanthanum nitrate hexahydrate ($La(NO_3)_3.6H2O$), scandium chloride ($ScCl_3$), europium chloride hexahydrate ($EuCl_3 \cdot 6H2O$), neodymium nitrate hexahydrate ($Nd(NO_3)_3.6H2O$), nitric acid concentrate and ICP standards of REEs were obtained from Sigma Aldrich. All the chemicals were of reagent grade and, therefore, no further purification was done before their use.

6.2.2 PREPARATION OF LDH

Mg/Al G.A. LDH was prepared by Mg and Al as divalent and trivalent ions, respectively, and G.A. as anion carrier. The mixed metal intercalation with G.A. was achieved by precipitating organic and inorganic phases by controlling pH of the solution. This in-situ synthesis was carried out by using Mg and Al nitrates in water, where G.A. was also added and stirred for a specified time. Co-precipitation occurred by controlling the pH levels in a basic medium and maintaining it at 10. Moreover, an ageing step was introduced to achieve a stable LDH structure.

Briefly, 2 grams of G.A. was dissolved in 100 ml of DI water with constant stirring at 70°C for an hour. A mixture of Mg and Al salts containing ratio of 3:1 as 0.75M $Mg(NO_3)_2 \cdot 6HO$ and 0.25M $Al(NO_3)_3 \cdot 9HO$, was slowly added in G.A. mixture and stirred for 120 min. To precipitate the LDH formed the pH of the solution was adjusted by drop wise addition of NaOH to maintain pH level at 10. The resulting solid precipitants were aged for 18 hours to get stable LDH structure and further centrifuged and washed several times with DI water and ethanol to ensure removal of any excess regents.

Similar procedure was performed with a 4:1 of Mg-Al and also G.A. percentage was varied as 2 and 5% solutions to check their effect over adsorption of REEs.

6.2.4 ADSORPTION AND REGENERATION PROCEDURE

Adsorption experiments were carried out in a sequence form preliminary tests to isothermal analysis. In preliminary test, the best ratio of Mg-AL and best percentage of G.A. was tested. Mg-AL ratio of 3:1 and 4:1 was tested and also G.A. concentration was varied in perceptive as 2% and 5%.

Estimating best adsorption results it is compulsory to check the pH effects of adsorption. Hence for this purpose, a pH test was run over a fixed dose and concentration and the results were compared. As REEs are often precipitated at a higher pH than neutral so the pH levels higher than 7 were not considered in the following study.

Prior to kinetic studies, a dose test was performed, which determined the best optimum dose for adsorption. For this purpose, adsorbent dose was varied from 1-15 mg/10ml of REEs solution. The graphical approach was used to locate the best dose where adsorption changed rapidly defined optimum dose point.

Kinetics studies were performed with optimum dose and pH with selective time periods. Adsorption test was preceded for kinetics to point where no considerable change in concentration as observed. This equilibrium point was found different for REEs and so different REEs were analysed differently for kinetics studies.

Adsorption isotherms were obtained by using the best-obtained parameters of pH, dose and time. The obtained results were analysed by Langmuir, Freundlich and Temkin isotherms and adsorption parameters were estimated.

For thermodynamic studies, 50 ppm solution of REEs over 10 mg adsorbent doses was stirred in a shaker at temperatures of 298, 308, 318 and 328 K. Form this heat content of adsorption and enthalpy of the system is obtained. The nature of adsorption was also determined based on the heat of reaction i.e. chemisorption or physisorption.

For desorption experiments after screening through different solvents, 0.1M HNO_3 was found to give considerable results for REEs desorption. An adsorbent sample containing REEs were treated with 0.1 M HNO_3 for a specified time. This treated sample was water washed and reused for adsorption-desorption for several cycles.

7. RESULTS AND DISCUSSIONS

7.1 CHARACTERISATION AND MORPHOLOGY OF MG-AL-G.A. LDH

The structure of Mg-Al LDH with different concentrations of G.A. was identified by XRD pattern shown below. Characteristic peaks were found on diffraction planes (h k l) at 003, 006, 009,012,018 and 110. The 2θ peak at diffraction plane (0 0 3) defines the basal spacing between the samples was increased by increasing gum concentration i.e. from 2.01 nm to 2.15 nm for G.A. 2% and 5%, respectively. This increase can be explained by the introduction of gum molecules into LDH structure where brucite sheets could form to certain angels producing an increment in basal spacing.

In the table below, some of the characteristic parameters for all the G.A. samples are given. From the results, it can be seen as a minor increase in the lattice parameter ‘a’ which refers to the distance in the octahedral O-O layer. Whereas, the lattice parameter ‘c’ referring to the interlayer distance, has been increased due to the presence of G.A. into LDH brucite sheets. Changes in diffraction planes at (0 0 3) is also noticeable, which explains the

exfoliation was achieved because the G.A. addition in brucite layer allowed laying or tilting to certain angles.

Table 5: XRD parameters of Mg-Al G.A. samples

Sample	**Lattice parameters**		**Interlayer thickness** (nm)	**Diffraction planes** (nm)					
	a(nm)	c(nm)		**d 003**	**d 006**	**d 009**	**d 012**	**d 018**	**d 110**
Mg-Al-G.A. 2	0.34	2.73	0.49	0.91	0.45	0.29	0.26	0.22	0.17
Mg-Al-G.A. 5	0.35	2.76	0.50	0.94	0.46	0.29	0.26	0.22	0.17

The FTIR spectra of prepared LDH samples are shown below. Adsorption peaks present at 3,700-3,200 cm^{-1} are due to the presence of O-H bond vibrations. Peaks below 800 cm^{-1} represent metallic bonds of Mg and Al i.e. Mg-O, O-Mg-O etc. Other bands gaps represent; 3,000-2,800 cm^{-1} corresponding CH_2 and CH_3 stretching, ~ 1,750 cm^{-1} corresponds to C-O covalent bonds, ~ 1,635 relates to C=O double bond, 1,200-1,050 cm^{-1} corresponds to C-O-C ether linkage, ~1,410 cm^{-1} and ~1,350 cm^{-1} are related to CH and CH_2 vibrations. Moreover, presence of these peaks confirms the presence of G.A. into LDH structure along with metals. The FTIR spectra conclude the successful modification and a successful loading of G.A. were obtained.

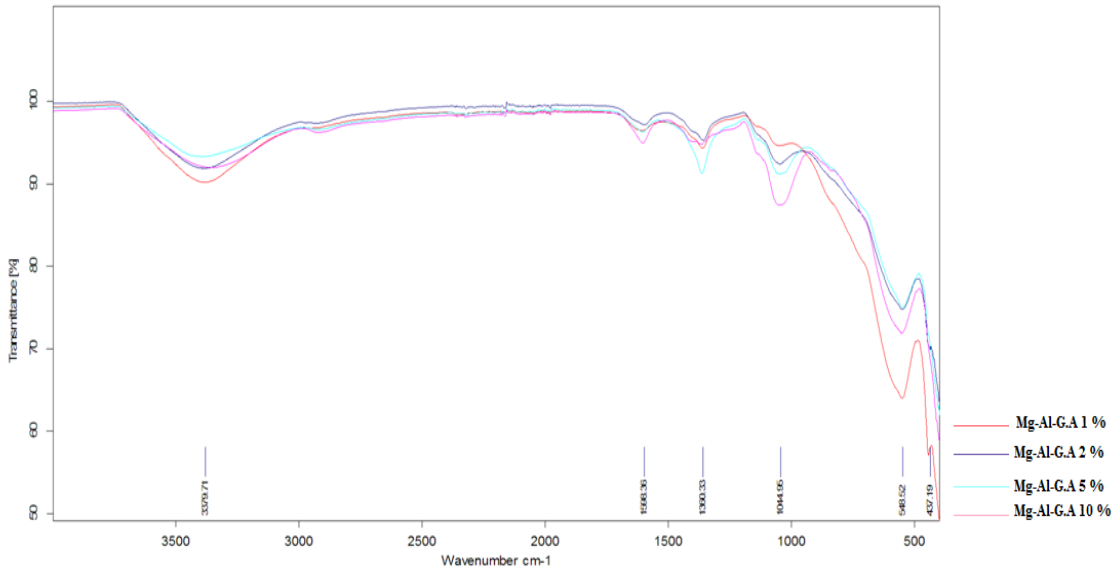

Figure 10: FTIR spectra of Mg-AL-G.A. 1, 2, 5, 10% LDH

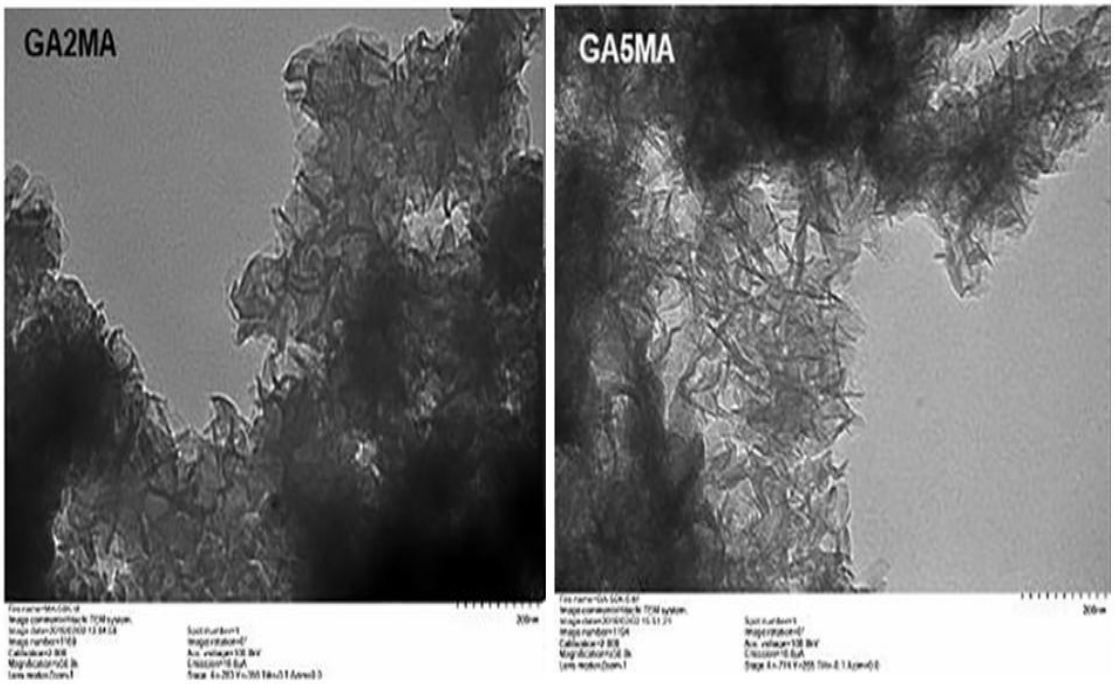

Figure 11: TEM micrographs of G.A. 2, 5% Mg-Al-G.A. LDH

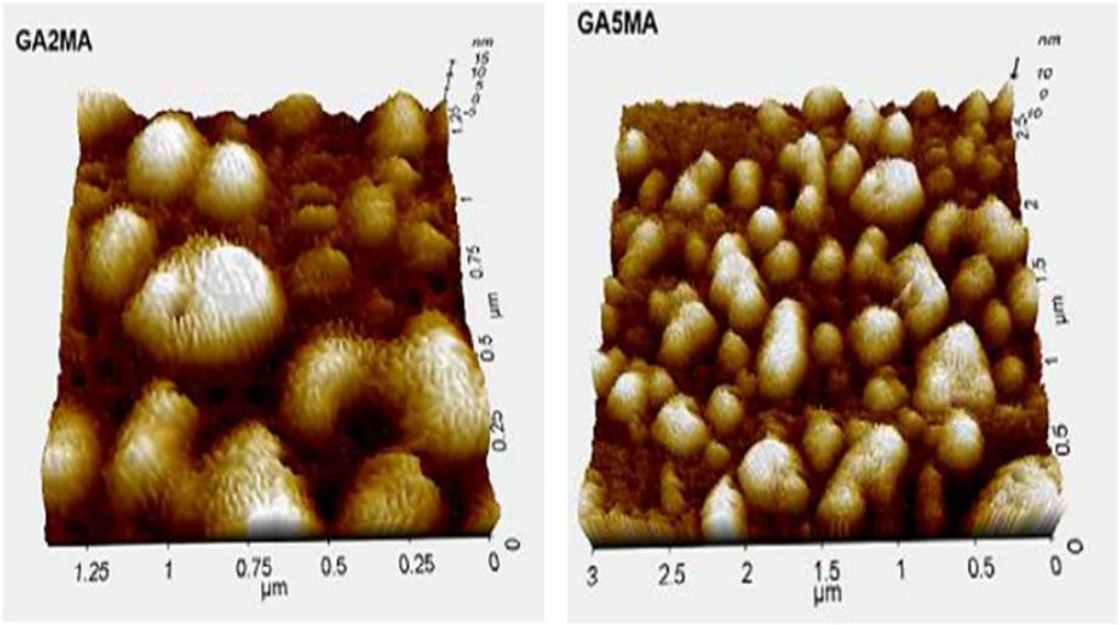

Figure 12: AFM images of G.A. 2, 5% Mg-Al-G.A. LDH

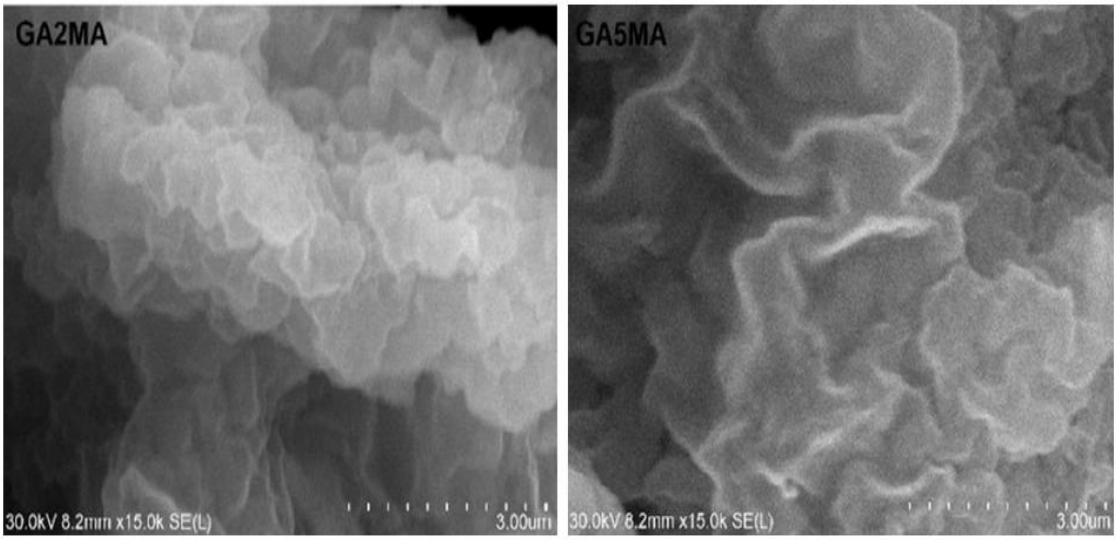

Figure 13: SEM images of G.A. 2, 5% Mg-Al-G.A. LDH

The microscopic graphs are obtained to study the morphology, particle size and their distribution over the whole substance. TEM images are presented above for G.A. 2% and 5% concentrations. These graphs illustrate irregular shaped fibrous morphology and a uniform distribution of LDH in G.A. matrix. It can be clearly seen that the degree of exfoliation is affected by the G.A. concentration and exfoliation increases with G.A. concentration.

AFM graphs are presented herein above which also confirms the morphology obtained through TEM. It can be seen in the AFM images that Mg-AL LDH forms a developed network and the formation of the crystal is monolithic due to the presence of Mg-AL-G.A. sheets all over the matrix. Sheet thickness was obtained at approx. 6-8 nm and the crystals were observed to be a mix of small particles. These AFM images clearly suggest that G.A. forms a shell-like structure around Mg-Al LDH layers which make the LDH particles bigger and heavier in size.

SEM images above shows that the Mg-Al LDH are non-uniformly devolved into the matrix of G.A. This non-uniformity and randomness show that the LDH molecules are stacked differently in every sheet and hence different size platelets are formed.

7.2 PRELIMINARY TEST

This preliminary test was performed before any detailed experiments to obtain the best Mg/Al ratio and also the percentage loading of G.A. The results from the experiments are shown in the graphs below. It can be observed that the Mg/Al ratio (3:1) give the best results for removal. This can be explained by the modification of the brucite layer charge density which affects the overall zeta potential and hence the adsorption of particles.

Figure 15 shows that, at a 5% concentration of G.A., maximum removal was observed. By further increment, the removal of REEs is not affected much.

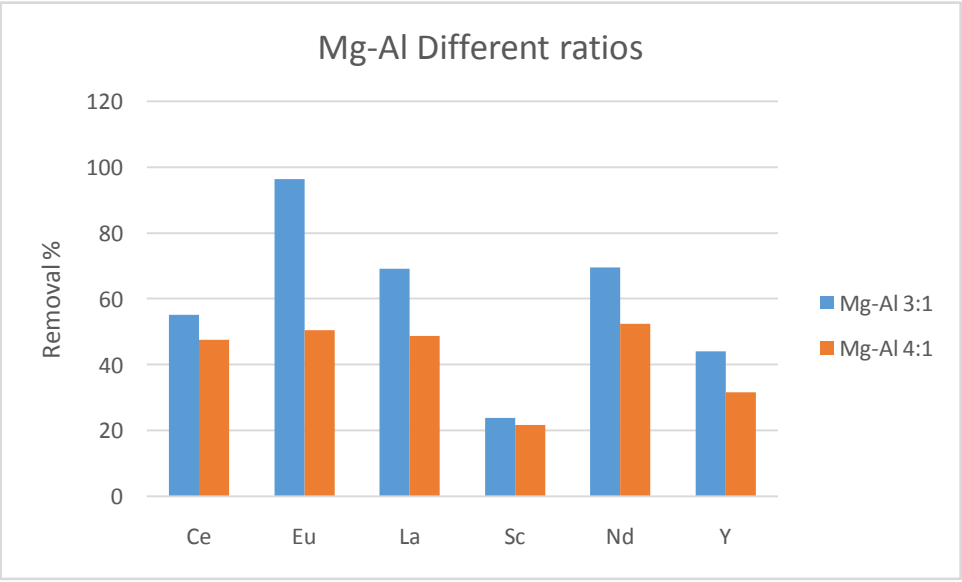

Figure 14: Effect of Mg/Al ratio over adsorption

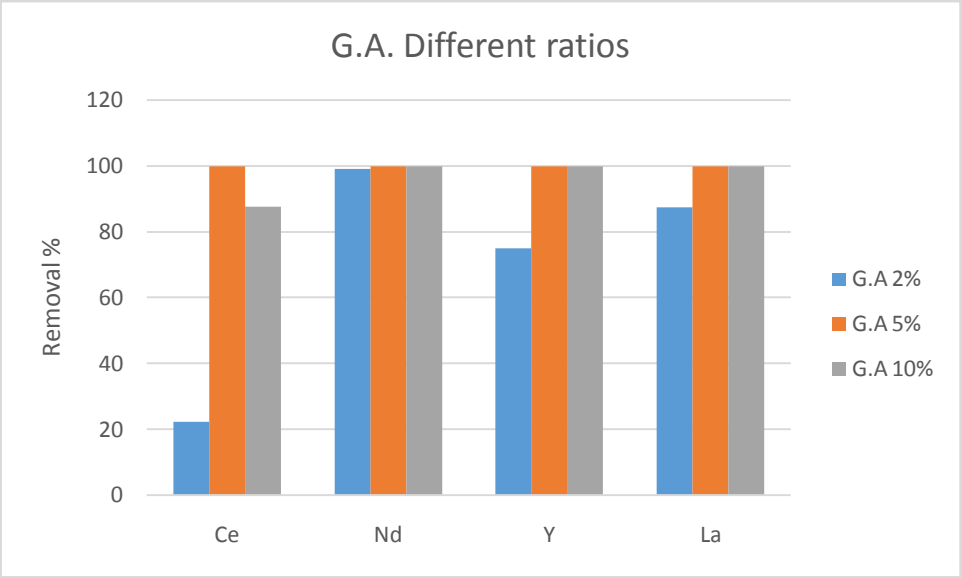

Figure 15: Effect of G.A. % in LDH towards the removal of REEs

7.3 EFFECT OF PH

The effect of pH largely affects any adsorption due to change in electrostatic attraction and repulsions. The effect of pH over adsorption was studied between pH 2 and pH 7. pH higher than 7 was not considered for the present study as the REEs solution might precipitate after pH 7. From the figure below, it can be observed that the adoption of REEs is increasing the function of pH. An increase in the adsorption of all the REEs is obtained by pH increment. This can be explained through the zeta potential curve below where ζ potential point is at pH_{ZPC} 2.65. Hence, when the pH is lower than this point, REEs face a repulsion form adsorbent surface due to the positive charge and also the competition of H^+ is also prominent. Nevertheless, an increase in pH after this pH_{ZPC} increases the overall adsorption. The point of optimum pH was obtained by noticing the sharp rise at pH 4, which was used in further studies.

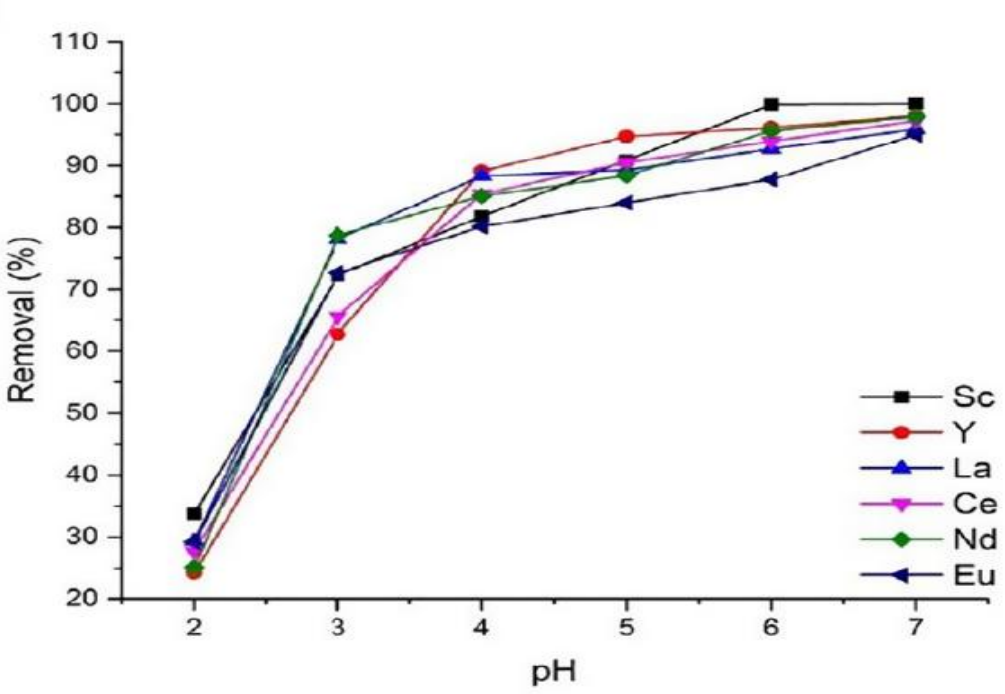

Figure 16: Effect of pH over REEs removal

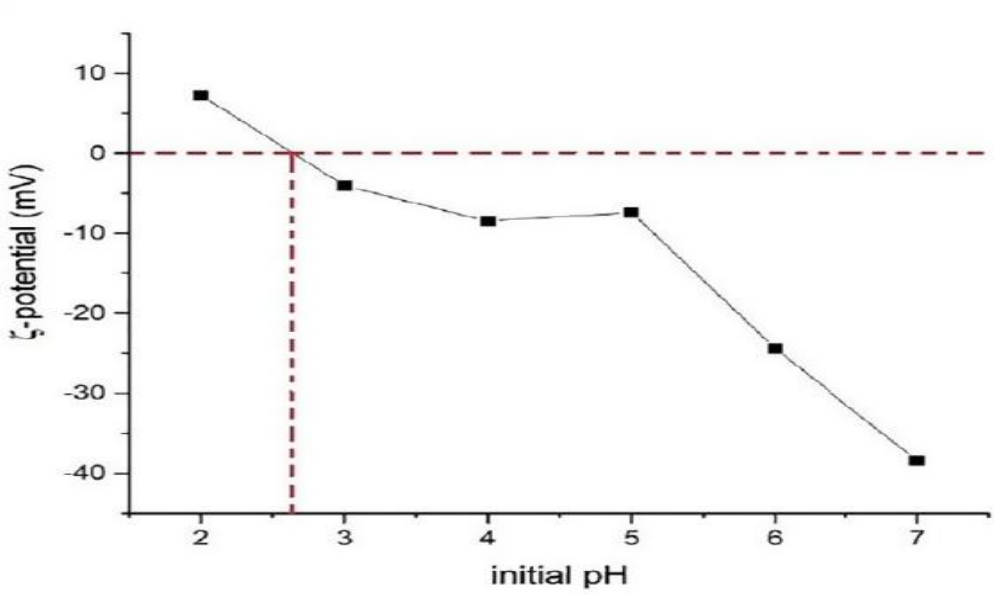

Figure 17: Zeta potential curve

7.4 EFFECT OF ADSORBENT DOSE

Effect of the dose from 1 mg to 15 mg/10 ml of REEs, is illustrated in the graph below. From the chart it can be noticed that an increase in the adsorbent dose causes an increase in

adsorption, which is mainly due to an increase of the adsorption sites. However, a sharp or rapid increase can be seen until 10mg and a further increase in dose affects only a fraction of removal. Thus, a dose of 10 mg/10 ml of REEs could be defined as the optimum dose and was used in further experiments.

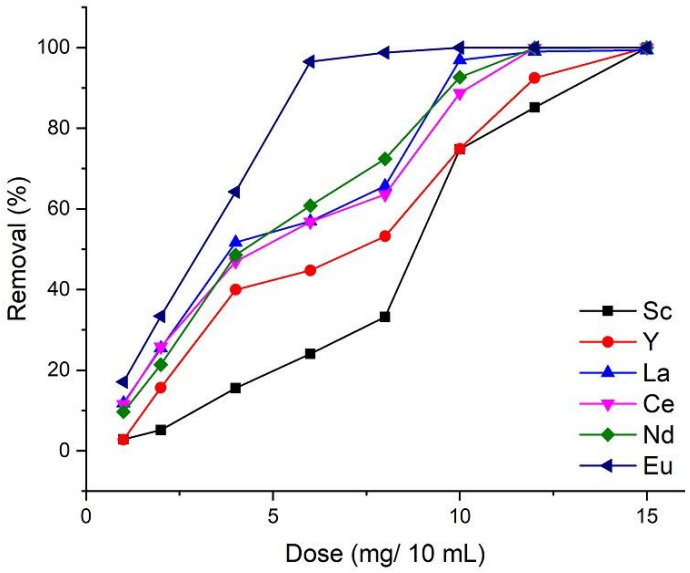

Figure 18: Effect of dose on REEs removal

7.5 KINETIC STUDIES

The figure below illustrates the effect of time on the adsorption of REEs over Mg-AL-G.A. LDH. It can be observed that the adsorption of REEs increases rapidly in the first 90 min period. After this period, adsorption reaches its dynamic equilibrium state and hence no major change in adsorption can be observed.

Kinetics models of adsorption were applied to all REEs and adsorption parameters were obtained with R^2 errors. These plots for pseudo first order, pseudo-second order, Boyd and intra-particle diffusion model are shown below, and the results of parameters are summarised in table 6.

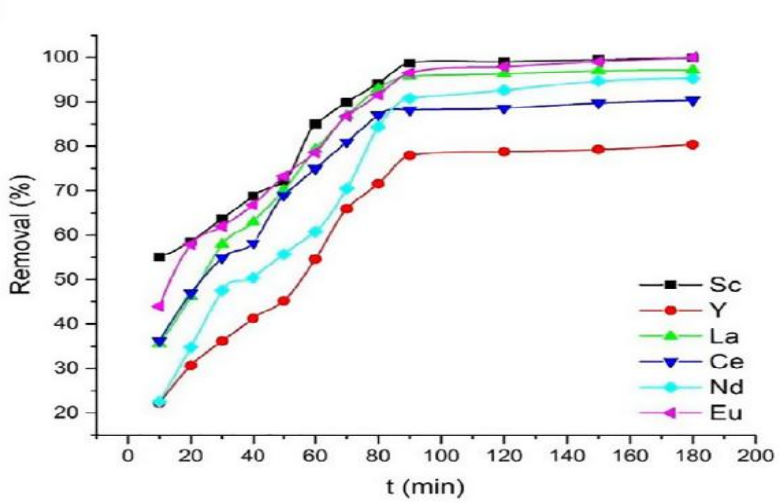

Figure 19: Effect of time on adsorption of REEs

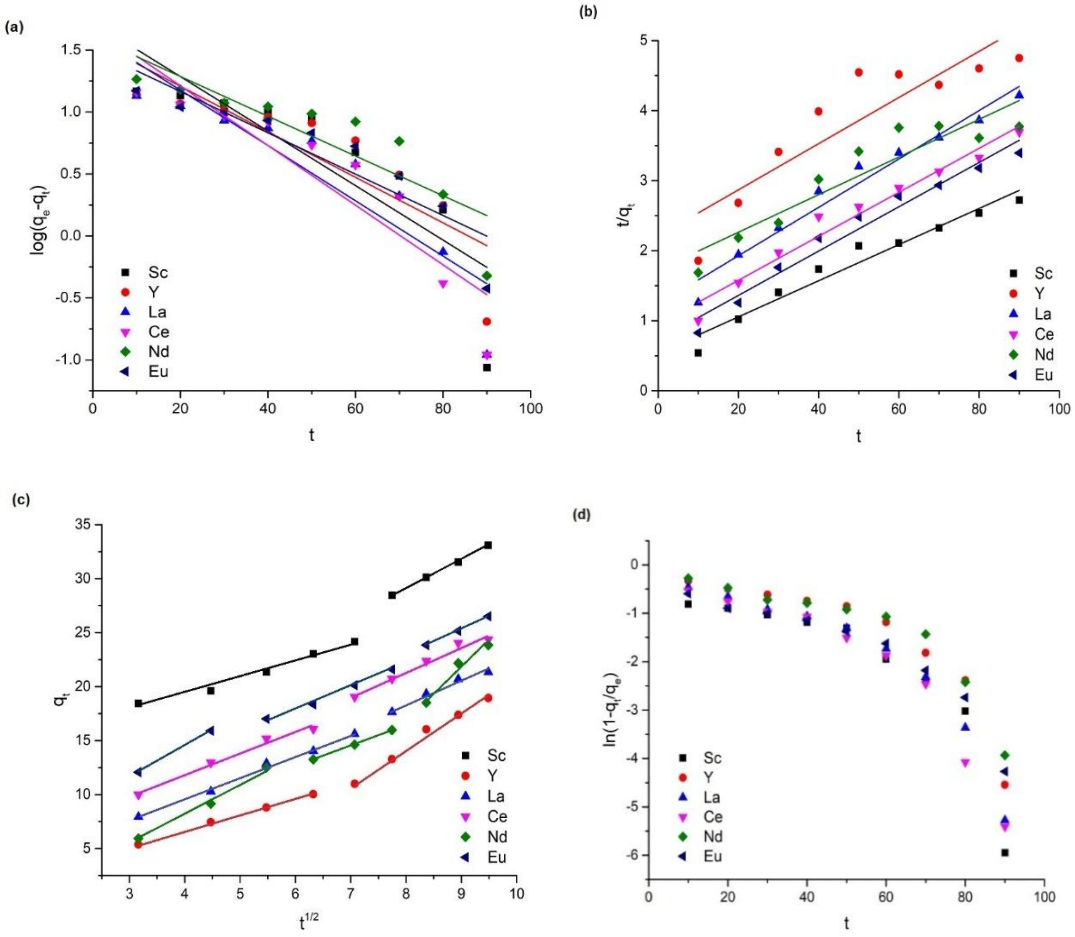

Figure 20: Model fitting curves of pseudo-first order (a); pseudo-second order (b); Intra-particle diffusion model (c); Boyd model (d)

The results from the kinetics suggest that the pseudo second-order determines the kinetics better than pseudo first as the R^2 error and the calculated values of capacities are closer to the experimental values. This also determines the chemical reactions control of the adsorption kinetics. Hence, chemisorption was determined to be the rate-limiting step for REEs adsorption.

The diffusion plots above determined that film diffusion is a rate controlling parameter. Three distinct linear regions in the plot(c) for Nd and Eu; explains a three-stage diffusion i.e. boundary layer, macropore and micropore, whereas the absence of the macropore diffusion in other REEs shows that only the boundary layer and micropore diffusions are significant to determine kinetics. Hence, based on the results, it can be concluded that the adsorption rate was affected by the chemical reactions with adsorbent and rates of diffusion of REEs through liquid films around adsorbent particles.

Table 6: Kinetic parameters of REEs adsorption over Mg-Al-G.A. LDH

REEs	**$q_e$exp (mg/g)**	**Pseudo First order**			**Pseudo Second Order**		
		$q_e$calc (mg/g)	**k_1 (min $^{-1}$)**	**R^2**	**$q_e$calc (mg/g)**	**k_2 (min $^{-1}$)**	**R^2**
Sc	33.16	53.21	5.0×10^{-2}	0.68	38.77	1.2×10^{-2}	0.95
Y	19.15	47.59	4.2×10^{-2}	0.71	23.28	0.8×10^{-2}	0.77
La	21.45	41.98	5.1×10^{-2}	0.79	28.95	0.9×10^{-2}	0.96
Ce	24.47	49.30	5.5×10^{-2}	0.82	26.74	1.4×10^{-2}	0.96
Nd	24.33	40.51	3.7×10^{-2}	0.73	27.13	0.8×10^{-2}	0.84
Eu	26.89	31.60	3.8×10^{-2}	0.1	31.61	1.3×10^{-2}	0.96

7.6 ISOTHERMAL ANALYSIS

The figure below illustrates the isotherms of REEs adsorption over Mg-AL-G.A. LDH. From the charts, it was noted that the adsorption of REEs per gram was an increasing function of concentration. Meaning that the over adsorption capacity was increased as the concentration of adsorbent was increased. This can be explained by the fact that, at low concentration, most of the adsorbent sites are empty which are filled when a higher concentration is introduced.

From fitting results (table 7), it was obtained that for all the REEs showed best fit with the Langmuir model and R^2 was minimised for all REEs except scandium. Hence, these REEs can be inferred to have monolayer adsorption over the LDH surface. Scandium, however, showed a better fit with Freundlich model which confirms a multilayer and heterogeneous adsorption due to the value of 'n>1'. The order of adsorption based on capacities can be concluded as: Sc> Y >Nd> Ce >Eu> La. The order of adsorption shows that; smaller ionic size has higher adsorption than of lower size. In table 8, the adsorption results from other studies are also presented as a comparison with the present study.

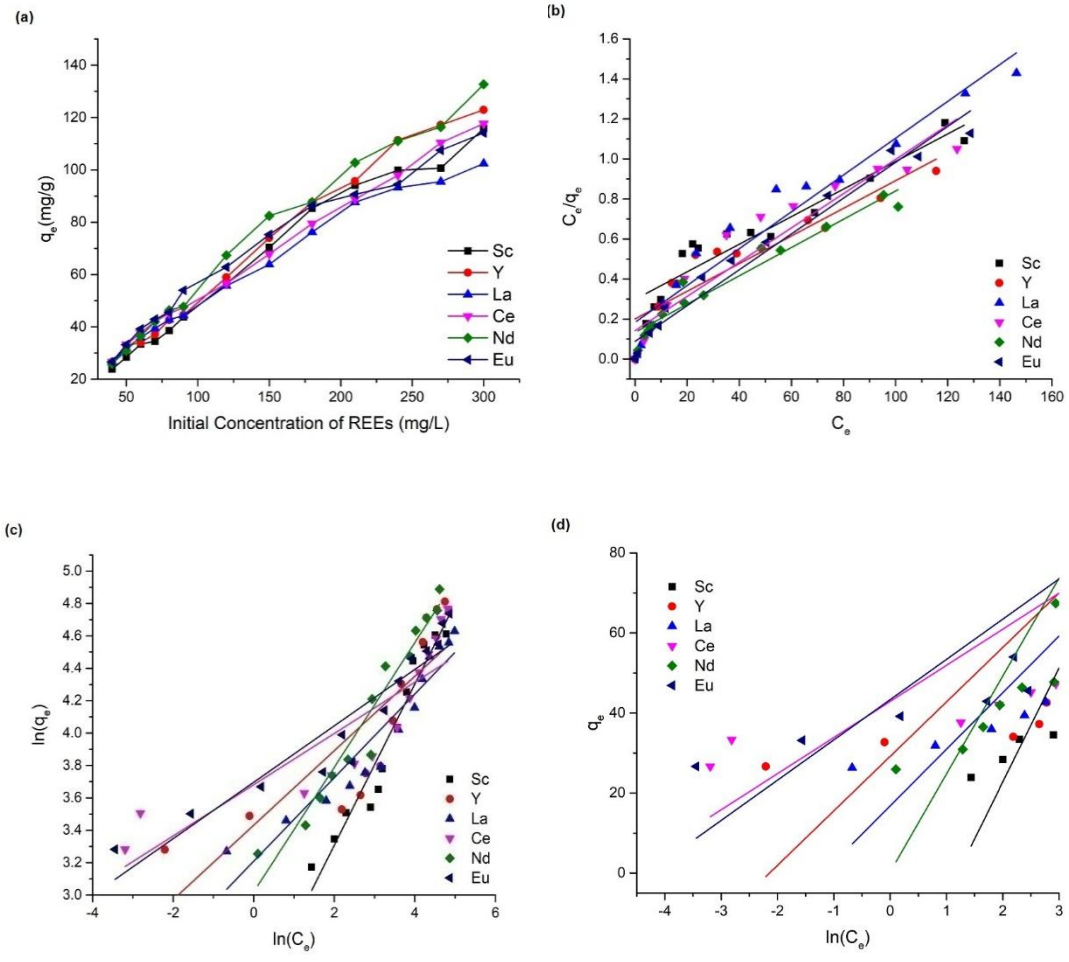

Figure 21: Effect of initial concentration on adsorption of REEs (a); Isothermal models of Langmuir, Freundlich and Temkin adsorption isotherms of REEs (b-d)

Table 7: Isotherms parameter for REEs adsorption over Mg-Al-G.A. LDH

REEs	Langmuir			Freundilich			Tempkin		
	Q_o (mg/g)	K_L (L/mg)	R_L^2	K_F (L/g)	n	R_F^2	A (L/g)	B (J/mol)	R_T^2
Sc	145.14	0.023	0.91	10.1	2.01	0.94	0.30	28.46	0.88
Y	144.72	0.034	0.84	30.90	4.34	0.68	8.51	13.61	0.55
La	108.69	0.05	0.94	24.75	3.87	0.89	3.28	14.14	0.78
Ce	116.82	0.06	0.90	39.68	6.32	0.74	114.97	9.01	0.59
Nd	141.44	0.053	0.94	20.46	2.59	0.94	1.01	24.48	0.87
Eu	111.73	0.102	0.97	40.30	5.74	0.88	74.41	10.05	0.75

Table 8: Comparison of adsorption capacity over different adsorbents

Adsorbent	Adsorption conditions	Adsorption Capacity (mg/g)						Reference
		Sc	Y	La	Ce	Nd	Eu	
Biochar from wood saw dust	C_o: 20 mg/L, Dose: 1 g/L, pH: 3	7.5	-	-	-	8.0	-	Komnitsas et al., (2017)
(SiO2/UF) composite material	C_o: 10^{-3} mol/L, Dose: 10 g/L, pH: 3	-	-	-	-	2.8	3.1	Naser et al., (2015)
Bone powder	C_o: 5-500 mg/L, Dose: 20 g/L, pH: N/A	-	-	8.43	-	10.75	12.6	Butnariu et al., (2015)
Mg-Fe-CO_3 LDH	C_o: 5000 mg/L, Dose: 10 g/L, pH: 1	-	-	480	-	192	-	Gasser and Aly (2013)

HPC-g-PAA/APT	C_o: 300 mg/L, Dose: 1 g/L, pH: 6	-	-	270	200	-	-	Zhu et al., (2015)
PAN mobilised SEP	C_o: 1 mg/L, Dose: 1 g/L, pH: 4	42.39	33.34	115	12.64	-	88.2	Ramasamy et al., (2017)
Mg-Al-G.A.	*C_o: 50 mg/L, Dose: 1 g/L, pH: 4*	*145.1*	*144.7*	*108.6*	*116.8*	*141.4*	*111.7*	*Present study*

7.7 THERMODYNAMIC ANALYSIS

The chart below shows the thermodynamic analysis of adsorption REEs over Mg-Al-G.A.-LDH. The relationship between lnKc and 1/T predicts a linear trend and hence the values of enthalpy, Gibbs free energy and entropy can be predicted from the graphs (table 9).The obtained values show that the adsorption phenomenon is spontaneous as the value of Gibbs free energy is found negative in all cases. The enthalpy of adsorption was positive and has a value higher than 50 kJ/mol which determines the endothermic and chemisorption nature of adsorption. The positive values of entropy confirm that the disorder during the adsorption is increased and also the capacity of adsorption increases as the temperature is increased.

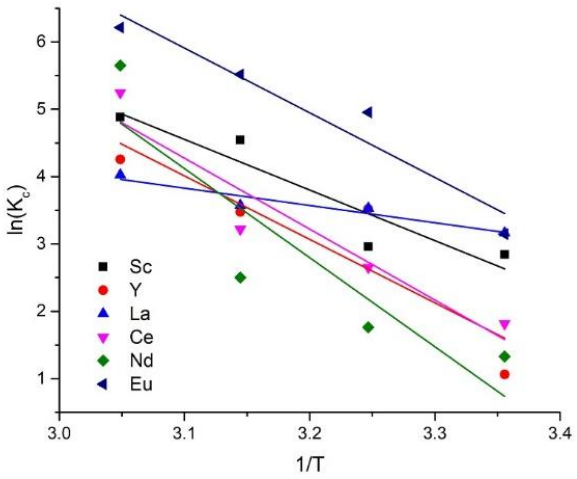

Figure 22: Temperature dependence of the adsorption for REEs

Table 9: Thermodynamic parameters of adsorption

REEs	ΔH^0 (kJ/mol)	ΔS^0 (J/mol/K)	ΔG^0 (kJ/mol)			
			293K	303K	313K	323K
Sc	62.49	231.56	7.05	7.58	-12.02	-13.32
Y	78.33	276.16	-2.63	-9.01	-9.19	-11.60
La	52.12	98.03	-7.84	-9.04	-9.45	-10.98
Ce	87.55	306.93	-4.5	-6.79	-8.51	-14.30
Nd	109.94	375.08	-3.29	-4.51	-6.61	-15.41
Eu	79.87	296.72	-7.79	-12.69	-14.59	-16.94

7.8 DESORPTION AND REUSE

Desorption capability of Mg-Al-G.A. LDH was tested over 0.1 M HNO_3 solutions for 8 cycles of adsorption. The results of these regeneration cycles are plotted below. The noticeable factor is the decrease of adsorption after each cycle which concludes that the adsorption capacity decreases after each cycle of regeneration. This decrease can be explained by the incomplete regeneration of adsorbed sites and also the surface damage by hydraulic forces. Nevertheless, with quite many adsorption cycles and reusability Mg-Al-G.A. LDH proves to be a potential adsorbent for REEs uptake.

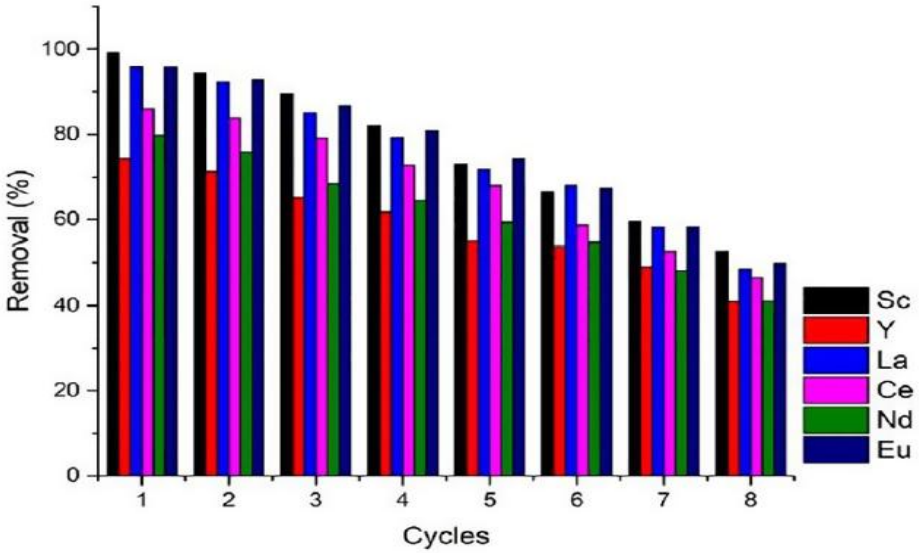

Figure 23: Desorption cycles of REEs over Mg.Al.G.A. LDH

8. CONCLUSIONS

Mg/Al G.A. LDH is a potential adsorbent for REEs uptake, which compared to other composite materials have much higher adsorption capacities. The presence of G.A. in LDH was confirmed with the FTIR spectra and by the increment in basal spacing with the introduction of G.A. into the LDH structure. Microscopic analysis showed an irregular shaped fibrous morphology and the formation of a shell-like structure around Mg-Al LDH layers by G.A. Experimental results yielded the optimum adsorption conditions as the Mg-Al ratio of (3:1), G.A. 5%, pH 4, dose 1 g/L and contact time of 90 min. Adsorption capacities of adsorbent over target REEs were: La 108.69 mg/g, Ce 116.82 mg/g, Nd 141.44 mg/g, Eu 111.73 mg/g, Sc 145.14 mg/g, and Y 144.72 mg/g. The order of adsorption based on capacities was concluded as: Sc> Y >Nd> Ce >Eu> La.

Conclusively, the adsorption results suggest that Mg-Al G.A. LDH has great affinity towards REEs and hence it can be used in applications such as column operations, wastewater treatment, REEs extraction from mineral ores etc. However, further studies must be conducted on the aspects of their strength properties and mechanical feasibilities for column operations. The aspects of loss in the LDH structure and metal leaching during the regeneration procedure must also be taken into account when applying them in large scale applications.

9. SUMMARY

The present study was conducted to find a suitable bio-degradable adsorbent for the removal of REEs from an aqueous media. In the course of the study, Mg-Al-G.A. LDH was found to uptake significant amounts of the REEs from the aqueous medium. The mixed metal intercalation with G.A. was achieved by precipitating organic and inorganic phases by controlling the pH of the solution. Six different REEs: La, Ce, Nd, Eu along with Sc and Y, were used to test the adsorption phenomenon on the novel adsorbent. In the research, the target REEs were tested to find the best parameters of pH, dose, time, concentration and temperature.

Adsorbent particles were characterised by analytical equipment i.e. XRD, FTIR, AFM, SEM, TEM and Zeta potential meter. The characterisation yielded that Mg-Al forms brucite sheets with G.A. and also the effect of G.A. modified the crystal structure of LDH. FTIR spectra confirmed presence of G.A. into the LDH structure. Microscopic images yielded that G.A. formed a shell-like structure around Mg-AL LDH layers and a non-uniform distribution of LDH matrix was obtained.

The experimental results yielded the optimum parameters as the Mg-Al ratio of (3:1), G.A. 5%, pH 4 and dose of 1g/L. The adsorption of REEs increased rapidly in the first 90 min period and, after this period, adsorption reached its equilibrium state. The results from kinetics suggested that the pseudo second order determined the kinetics better than the pseudo first as the R^2 error and the calculated values of capacities are closer to the experimental values. This also determined the chemical reactions controlled by the adsorption kinetics.

From isothermal analysis, it was noted that the adsorption of REEs per gram was increasing the function of the concentration. Fitting results showed that all the REEs were fitted with the Langmuir model except scandium. Scandium, however, showed a better fit with the Freundlich model which confirmed a multilayer and heterogeneous adsorption due to the value of ‘n>1’. The adsorption capacities of adsorbent over target REEs are: La 108.69 mg/g, Ce 116.82 mg/g, Nd 141.44 mg/g, Eu 111.73 mg/g, Sc 145.14 mg/g and Y 144.72 mg/g. The order of adsorption based on capacities was concluded as: Sc> Y >Nd> Ce >Eu> La.

Thermodynamic analysis showed that adsorption was spontaneous, and the value of Gibbs free energy was found to be negative in all cases. The enthalpy of adsorption was positive and had a value higher than 50 kJ/mol which determined the endothermic and chemisorption nature of adsorption. The positive values of entropy confirmed the disorder during the adsorption was increased and the capacity of adsorption increased as the temperature was increased.

The desorption of REEs from the adsorbent surface was obtained by using 0.1 M HNO_3 solution. The reusability of adsorbent was studied until 8 batch cycles and it was obtained that the adsorption sites start to decrease, resulting in a decrease in overall adsorption with the course of every cycle.

Conclusively, Mg-AL-G.A. LDH could be utilised as an efficient adsorbent for removing REEs form aqueous media. Future applications of the novel adsorbent could be found in column separation or wastewater treatment plants. However, further research must be conducted to find the applicability of adsorbent in industrial applications, and the loss of adsorbent during desorption cycles must be taken into account.

10. REFERENCES

Ali, O.I.M., Osman, H.H., Sayed, S.A. and Shalabi, M.E.H., 2011. The removal of some rare earth elements from their aqueous solutions on by-pass cement dust (BCD). *Journal of hazardous materials*, *195*, pp.62-67.

Anagnostopoulos, V.A. and Symeopoulos, B.D., 2013. Sorption of europium by malt spent rootlets, a low costbiosorbent: effect of pH, kinetics and equilibrium studies. *Journal of Radioanalytical and Nuclear Chemistry*, *295*(1), pp.7-13.

Anastopoulos, I., Bhatnagar, A. and Lima, E.C., 2016. Adsorption of rare earth metals: A review of recent literature. *Journal of Molecular Liquids*, *221*, pp.954-962.

Azzaoui, K., Hammouti, B., Lamhamdi, A., Mejdoubi, E. and Berrabah, M., 2015. The Gum Arabic in the southern region of Morocco. *Moroccan Journal of Chemistry*, *3*(1), pp.3-1.

Banerjee, S.S. and Chen, D.H., 2007. Fast removal of copper ions by gum arabic modified magnetic nano-adsorbent. *Journal of hazardous materials*, *147*(3), pp.792-799.

Barik, P., Bhattacharjee, A. and Roy, M., 2015. Preparation, characterization and electrical study of gum arabic/ZnO nanocomposites. *Bulletin of Materials Science*, *38*(6), pp.1609-1616.

Bartell, F.E., Thomas, T.L. and Fu, Y., 1951. Thermodynamics of Adsorption from Solutions. IV. Temperature Dependence of Adsorption. The Journal of Physical Chemistry, 55(9), pp.1456-1462.

Butler, C.L. and Cretcher, L.H., 1929. THE COMPOSITION OF GUM ARABIC1, 2. *Journal of the American Chemical Society*, *51*(5), pp.1519-1525.

Butnariu, M., Negrea, P., Lupa, L., Ciopec, M., Negrea, A., Pentea, M., Sarac, I. and Samfira, I., 2015. Remediation of rare earth element pollutants by sorption process using organic natural sorbents. *International journal of environmental research and public health*, *12*(9), pp.11278-11287.

Cadogan, E.I., Lee, C.H., Popuri, S.R. and Lin, H.Y., 2014. Efficiencies of chitosan nanoparticles and crab shell particles in europium uptake from aqueous solutions through biosorption: synthesis and characterization. *International Biodeterioration& Biodegradation*, *95*, pp.232-240.

Castor, S.B. and Hedrick, J.B., 2006. Rare earth elements. *Industrial minerals volume, 7th edition: Society for mining, metallurgy, and exploration, Littleton, Colorado*, pp.769-792.

Chen, S., Xu, Z., Zhang, Q., Lu, G., Hao, Z. and Liu, S. (2009). Studies on adsorption of phenol and 4-nitrophenol on MgAl-mixed oxide derived from MgAl-layered double hydroxide. *Separation and Purification Technology*, 67(2), pp.194-200.

Chiou, C.T., 2003. *Partition and adsorption of organic contaminants in environmental systems*. John Wiley & Sons.

Costantino U, Marmottini F, Nocchetti M, Vivani R (1998) Eur J InorgChem 1439

D.L. Ramasamy, V. Puhakka, E. Repo, S. Khan, M. Sillanpää, Coordination and silica surface chemistry of lanthanides (III), scandium (III) and yttrium (III) sorption on 1-(2-pyridylazo)-2-napththol (PAN) and acetylacetone (acac) immobilized gels,Chem. Eng. J. 324 (2017) 104–112.

Das, N. and Das, D., 2013. Recovery of rare earth metals through biosorption: an overview. *Journal of Rare Earths*, *31*(10), pp.933-943.

Dubey, S.S. and Rao, B.S., 2011. Removal of cerium ions from aqueous solution by hydrous ferric oxide–a radiotracer study. *Journal of hazardous materials*, *186*(2-3), pp.1028-1032.

Education.jlab.org. (2018). *It's Elemental - The Periodic Table of Elements* [online] Available at: http://education.jlab.org/itselemental/ [Accessed 10 Aug. 2018].

Foo, K.Y. and Hameed, B.H., 2010. Insights into the modeling of adsorption isotherm systems. *Chemical engineering journal*, *156*(1), pp.2-10.

Galhoum, A.A., Mahfouz, M.G., Gomaa, N.A., Abdel-Rehem, S.S., Atia, A.A., Vincent, T. and Guibal, E., 2015. Cysteine-functionalized chitosan magnetic nano-based particles for the recovery of uranium (VI): Uptake kinetics and sorption isotherms. *Separation Science and Technology*, *50*(18), pp.2776-2789.

Gambogi J., 2016, Rare Earths- Minerals year book: U.S. Geological Survey Scientific Investigations.

Gasser, M. and Aly, M. (2013). Separation and recovery of rare earth elements from spent nickel–metal-hydride batteries using synthetic adsorbent. *International Journal of Mineral Processing*, 121, pp.31-38.

Gładysz-Płaska, A., Majdan, M. and Grabias, E., 2014. Adsorption of La, Eu and Lu on raw and modified red clay. *Journal of Radioanalytical and Nuclear Chemistry*, *301*(1), pp.33-40.

Gok, C., 2014. Neodymium and samarium recovery by magnetic nano-hydroxyapatite. *Journal of Radioanalytical and Nuclear Chemistry*, *301*(3), pp.641-651.

Goonan T.G., 2011, Rare earth elements—End use and recyclability: U.S. Geological Survey Scientific Investigations Report 2011–5094, 15 p. available only at http://pubs.usgs.gov/sir/2011/5094/.

Granados-Correa, F., Vilchis-Granados, J., Jiménez-Reyes, M. and Quiroz-Granados, L.A., 2012. Adsorption behaviour of La (III) and Eu (III) ions from aqueous solutions by hydroxyapatite: kinetic, isotherm, and thermodynamic studies. *Journal of Chemistry*, *2013*.

Gupta, C. and Krishnamurthy, N. (2005). *Extractive metallurgy of rare earths*. Boca Raton: CRC.

He J., Wei M., Li B., Kang Y., Evans D.G., Duan X. Preparation of Layered Double Hydroxides. In: Duan X., Evans D.G. (eds) Layered Double Hydroxides. Structure and Bonding, vol 119. Springer, Berlin, Heidelberg

He, J., Wei, M., Li, B., Kang, Y., Evans, D. and Duan, X. (n.d.). Preparation of Layered Double Hydroxides. *Layered Double Hydroxides*, pp.89-119.

Hedrick, J. (2018). *USGS Minerals Information: Rare Earths*. [online] Minerals.usgs.gov. Available at: http://minerals.usgs.gov/minerals/pubs/commodity/rare_earths/ [Accessed 10 Aug. 2018].

Heraldy, E. and Nugrahaningtyas, K.D., 2017, February. X-ray Diffraction Analysis on Post Treatment of Ca-Mg-Al-Layered Double Hydroxide Slurry. In *IOP Conference Series: Materials Science and Engineering* (Vol. 176, No. 1, p. 012020). IOP Publishing.

Hussein Al Ali, S., Hussein, M., Hussein Al Ali, S., Zainal, Z., Nazrul-Hakim, M., Ismail, M. and Al-Qubaisi, M. (2012). Comparative study of Mg/Al- and Zn/Al-layered double hydroxide-perindopril erbumine nanocomposites for inhibition of angiotensin-converting enzyme. *International Journal of Nanomedicine*, p.4251.

Iftekhar, S., Srivastava, V. and Sillanpää, M. (2017). Synthesis and application of LDH intercalated cellulose nanocomposite for separation of rare earth elements (REEs). *Chemical Engineering Journal*, 309, pp.130-139.

Iftekhar, S., Srivastava, V. and Sillanpää, M., 2017. Enrichment of lanthanides in aqueous system by cellulose based silica nanocomposite. *Chemical Engineering Journal*, *320*, pp.151-159.

Iftekhar, S., Srivastava, V. and Sillanpää, M., 2017. Synthesis and application of LDH intercalated cellulose nanocomposite for separation of rare earth elements (REEs). *Chemical Engineering Journal*, *309*, pp.130-139.

Kameda, T., Kondo, E. and Yoshioka, T. (2014). Equilibrium and kinetic studies of Se(vi) removal by Mg–Al layered double hydroxide doped with Fe2+. *RSC Adv.*, 4(106), pp.61817-61822.

Kameda, T., Oba, J. and Yoshioka, T. (2015). Kinetics and equilibrium studies on Mg–Al oxide for removal of fluoride in aqueous solution and its use in recycling. *Journal of Environmental Management*, 156, pp.252-256.

Kameda, T., Oba, J. and Yoshioka, T. (2018). *Recyclable Mg–Al layered double hydroxides for fluoride removal: Kinetic and equilibrium studies*.

Kameda, T., Saito, M. and Umetsu, Y., 2006. Preparation and characterisation of Mg–Al layered double hydroxides intercalated with 2-naphthalene sulphonate and 2, 6-naphthalene disulphonate. *Materials transactions*, *47*(3), pp.923-930.

Khalfaoui, M., Knani, S., Hachicha, M.A. and Lamine, A.B., 2003. New theoretical expressions for the five adsorption type isotherms classified by BET based on statistical physics treatment. *Journal of colloid and interface science*, *263*(2), pp.350-356.

Khan, A.A. and SINGI, R., 1987. Adsorption Thermodynamics of Carbofuran on Sn (IV) Arsenosilicate in H*, Na* and Ca^* Forms. *DEDICATED TO MV EVER LOViNQ FATHER LATE SHRl CH ATTRA PAL SIN6H*, p.197.

Khotimchenko, M., Kovalev, V., Khozhaenko, E. and Khotimchenko, R., 2015. Removal of yttrium (III) ions from water solutions by alginate compounds. *International journal of environmental science and technology*, *12*(10), pp.3107-3116.

Komnitsas, K., Zaharaki, D., Bartzas, G. and Alevizos, G. (2017). Adsorption of Scandium and Neodymium on Biochar Derived after Low-Temperature Pyrolysis of Sawdust. Minerals, 7(10), p.200.

Kumar S., Senthamarai N. et al., 2014. Adsorption kinetics, mechanism, isotherm, and thermodynamic analysis of copper ions onto the surface modified agricultural waste. Environ. Prog. Sustainable Energy, 33: 29–32.

Li, F. and Duan, X. (n.d.). Applications of Layered Double Hydroxides. *Layered Double Hydroxides*, pp.193-223.

Lyubchik, S.I., Lyubchik, A.I., Galushko, O.L., Tikhonova, L.P., Vital, J., Fonseca, I.M. and Lyubchik, S.B., 2004. Kinetics and thermodynamics of the Cr (III) adsorption on the activated carbon from co-mingled wastes. *Colloids and Surfaces A: Physicochemical and Engineering Aspects*, *242*(1-3), pp.151-158.

Minerals.usgs.gov. (2018). *Historical Statistics for Mineral Commodities in the United States, Data Series 2005-140*. [online] Available at: http://minerals.usgs.gov/ds/2005/140/ [Accessed 10 Aug. 2018].

Morris, M.C., McMurdie, H.F., Evans, E.H., Paretzkin, B., Hubbard, C.R. and Carmel, S.J., 1980. Standards X-ray diffraction powder patterns. Section 17: Data for 54 substances. *Final Report National Bureau of Standards, Washington, DC. National Measurement Lab.*

Nalawade, P., Aware, B., Kadam, V.J. and Hirlekar, R.S., 2009. Layered double hydroxides: A review.

Naser, A.A., El-deen, G.S., Bhran, A.A., Metwally, S.S. and El-Kamash, A.M., 2015. Elaboration of impregnated composite for sorption of europium and neodymium ions from aqueous solutions. *Journal of Industrial and Engineering Chemistry*, *32*, pp.264-272.

Osman, M.E., Williams, P.A., Menzies, A.R. and Phillips, G.O., 1993. Characterization of commercial samples of gum arabic. *Journal of Agricultural and food chemistry*, *41*(1), pp.71-77.

Pubs.usgs.gov. (2018). *Scientific Investigations Report 2011–5094*. [online] Available at: http://pubs.usgs.gov/sir/2011/5094/ [Accessed 10 Aug. 2018].

Qiu, H., Lv, L., Pan, B.C., Zhang, Q.J., Zhang, W.M. and Zhang, Q.X., 2009. Critical review in adsorption kinetic models. *Journal of Zhejiang University-Science A*, *10*(5), pp.716-724.

Ramasamy, D.L., Khan, S., Repo, E. and Sillanpää, M., 2017. Synthesis of mesoporous and microporous amine and non-amine functionalized silica gels for the application of rare earth elements (REE) recovery from the waste water-understanding the role of pH, temperature, calcination and mechanism in Light REE and Heavy REE separation. *Chemical Engineering Journal*, *322*, pp.56-65.

Ramasamy, D.L., Puhakka, V., Repo, E., Khan, S. and Sillanpää, M., 2017. Coordination and silica surface chemistry of lanthanides (III), scandium (III) and yttrium (III) sorption on 1-(2-pyridylazo)-2-napththol (PAN) and acetylacetone (acac) immobilized gels. *Chemical Engineering Journal*, *324*, pp.104-112.

Ramasamy, D.L., Repo, E., Srivastava, V. and Sillanpää, M., 2017. Chemically immobilized and physically adsorbed PAN/acetylacetone modified mesoporous silica for the recovery of rare earth elements from the waste water-comparative and optimization study. *Water research*, *114*, pp.264-276.

Renaudin G, Francois M, Evrard O (1999) Cement Concrete Res 29:63

Ribeiro, F.W.M., Laurentino, L.D.S., Alves, C.R., Bastos, M.D.S.R., Costa, J.M.C.D., Canuto, K.M. and Furtado, R.F., 2015. Chemical modification of gum arabic and its application in the encapsulation of C ymbopogoncitratus essential oil. *Journal of Applied Polymer Science*, *132*(8).

Roosen, J. and Binnemans, K., 2014. Adsorption and chromatographic separation of rare earths with EDTA-and DTPA-functionalized chitosan biopolymers. *Journal of Materials Chemistry A*, *2*(5), pp.1530-1540.

Rsc.org. (2018). *Periodic Table – Royal Society of Chemistry*. [online] Available at: http://www.rsc.org/periodic-table [Accessed 10 Aug. 2018].

S. Iftekhar, V. Srivastava, M. Sillanpää, Enrichment of lanthanides in aqueous system by cellulose based silica nanocomposite, Chem. Eng. J. 320 (2017) 151–159.

S. Iftekhar, V. Srivastava, M. Sillanpää, Synthesis and application of LDH intercalated cellulose nanocomposite for separation of rare earth elements (REEs), Chem. Eng. J. 309 (2017) 130–139.

S. Iftekhar, V. Srivastava, S.B. Hammouda, M. Sillanpää, Fabrication of novel metal ion imprinted xanthan gum-layered double hydroxide nanocomposite for adsorption of Rare Earth Elements, Carbohyd. Polym., 2018 (in press Accepted Manuscript).

Shan, R., Yan, L., Yang, K., Hao, Y. and Du, B. (2018). *Adsorption of Cd(II) by Mg–Al–CO3- and magnetic Fe3O4/Mg–Al–CO3-layered double hydroxides: Kinetic, isothermal, thermodynamic and mechanistic studies*.

Srivastava, V., Sharma, Y.C. and Sillanpää, M., 2015. Green synthesis of magnesium oxide nanoflower and its application for the removal of divalent metallic species from synthetic wastewater. *Ceramics International*, *41*(5), pp.6702-6709.

Stutzman, P.E., 1996. *Guide for X-ray powder diffraction analysis of Portland cement and clinker*. US Department of Commerce, Technology Administration, National Institute of Standards and Technology, Office of Applied Economics, Building and Fire Research Laboratory.

Sun, X., Luo, H., Mahurin, S.M., Dai, S., Liu, R., Hou, X. and Dai, S., 2016. The adsorption of rare earth ions using carbonized polydopaminenano shells. *Journal of Rare Earths*, *34*(1).

Tan, X., Liu, S., Liu, Y., Gu, Y., Zeng, G., Cai, X., Yan, Z., Yang, C., Hu, X. and Chen, B. (2016). One-pot synthesis of carbon supported calcined-Mg/Al layered double hydroxides for antibiotic removal by slow pyrolysis of biomass waste. *Scientific Reports*, 6(1).

Theiss, F., Ayoko, G. and Frost, R. (2016). ChemInform Abstract: Synthesis of Layered Double Hydroxides Containing Mg2+, Zn2+, Ca2+and Al3+Layer Cations by Co-Precipitation Methods - A Review. *ChemInform*, 47(33).

Tong, X., Yang, Z., Xu, P., Li, Y. and Niu, X. (2017). Nitrate adsorption from aqueous solutions by calcined ternary Mg-Al-Fe hydrotalcite. *Water Science and Technology*, 75(9), pp.2194-2203.

V. Katiyar, N. Gerds, C.B. Koch, J. Risbo, H.C.B. Hansen, D. Plackett, Poly l-lactide layered double hydroxide nanocomposites via in situ polymerization of l-lactide, Polym. Degrad. Stab. 95 (2010) 2563–2573.

Van Gosen, B., Verplanck, P., Long, K., Gambogi, J. and Seal, R. (2018). *The rare-earth elements: Vital to modern technologies and lifestyles*.

Voncken, J. (n.d.). *The Rare Earth Elements*.

Wang, F., Zhao, J., Wei, X., Huo, F., Li, W., Hu, Q. and Liu, H., 2014. Adsorption of rare earths (III) by calcium alginate–poly glutamic acid hybrid gels. *Journal of Chemical Technology & Biotechnology*, *89*(7), pp.969-977.

Weber, R.J. and Reisman, D.J., 2012. Rare earth elements: A review of production, processing, recycling, and associated environmental issues. *US EPA Region*.

Xin, X., Si, W., Yao, Z., Feng, R., Du, B., Yan, L. and Wei, Q., 2011. Adsorption of benzoic acid from aqueous solution by three kinds of modified bentonites. *Journal of colloid and interface science*, *359*(2), pp.499-504.

Yao, T., Xiao, Y., Wu, X., Guo, C., Zhao, Y. and Chen, X., 2016. Adsorption of Eu (III) on sulfonated graphene oxide: Combined macroscopic and modeling techniques. *Journal of Molecular Liquids*, *215*, pp.443-448.

Younis, A.M., Kolesnikov, A.V. and Desyatov, A.V., 2014. Efficient removal of La (III) and Nd (III) from aqueous solutions using carbon nanoparticles. *American Journal of Analytical Chemistry*, *5*(17), p.1273.

Zhang, D., Zhao, G., Yu, J., Yan, T., Zhu, M. and Jiao, F. (2016). Thermodynamic and kinetic studies of effective adsorption of 2,4,6-trichlorophenol onto calcine Mg/Al-CO3 layered double hydroxide. *Journal of Wuhan University of Technology-Mater. Sci. Ed.*, 31(6), pp.1211-1218.

Zhao, F., Repo, E., Meng, Y., Wang, X., Yin, D. and Sillanpää, M., 2016. An EDTA-β-cyclodextrin material for the adsorption of rare earth elements and its application in preconcentration of rare earth elements in seawater. *Journal of colloid and interface science*, *465*, pp.215-224.

Zhu, Y., Zheng, Y. and Wang, A., 2015. A simple approach to fabricate granular adsorbent for adsorption of rare elements. International journal of biological macromolecules, 72, pp.410-420.